

**Characterization of surface treated layers on Austenitic Stainless Steel and
9.3%Cr Ferritic steel resulting from High Temperature Nitriding**

By

Muhammad Afiq Bin Mansor

Dissertation submitted in partial fulfilment of
the requirements for the
Bachelor of Engineering (Hons)
(Mechanical Engineering)

SEPTEMBER 2011

Universiti Teknologi PETRONAS
Bandar Seri Iskandar
31750 Tronoh
Perak Darul Ridzuan

CERTIFICATION OF APPROVAL

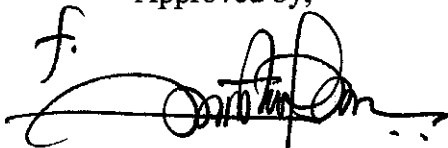
**Characterization of surface treated layers on Austenitic Stainless Steel and
9.3%Cr Ferritic steel resulting from High Temperature Nitriding**

By

Muhammad Afiq bin Mansor

A project dissertation submitted to the
Mechanical Engineering Programme
Universiti Teknologi PETRONAS
in partial fulfilment of the requirement for the
BACHELOR OF ENGINEERING (Hons)
(MECHANICAL ENGINEERING)

Approved by,



(Assoc. Prof Dr. Patthi Hussain)

UNIVERSITI TEKNOLOGI PETRONAS

TRONOH, PERAK

September 2011

CERTIFICATION OF ORIGINALITY

This is to certify that I am responsible for the work submitted in this project, that the original work is my own except as specified in the references and acknowledgements, and that the original work contained herein have not been undertaken or done by unspecified sources or persons.



MUHAMMAD AFIQ BIN MANSOR

ABSTRACT

The paper presents the results of investigation into corrosion resistance behaviour of gas nitrided 316L austenitic stainless steel and 9.3%Cr ferritic steel. Gas nitriding is a heat treatment technique that improved fatigue life, strength and wears and localized corrosion resistance. However, at certain temperature the steel becomes sensitized to possible intergranular corrosion. The heat treatment permits the formation to small precipitate particles of chromium carbide, $Cr_{23}C_6$ by reaction between the chromium and carbon in the material. During the heat treatment process, the samples are heated at two different temperatures for two samples which are at $600^{\circ}C$ and $900^{\circ}C$ in a tube furnace through which nitrogen gas is allowed to pass. The nitrogen reacts with the steel penetrating the surface to form nitrides. In order to investigate the presence of chromium carbide in grain boundary, further studies were conducted to analyse the microstructure, physical and mechanical properties by comparing the specimens before and after the nitriding process.

ACKNOWLEDGEMENTS

A million thanks to AP Dr Dr Patthi Bin Hussain, my supervisor who has given me many advices, opinions and guides in completion of this project. I really appreciate the time you allocate for me, to sit and discuss the problems that I had faced along the way. You always encourage me and that is what keeps me going and have belief in myself. Each time I came asking for your advice, my problems soothes bit by bit. Thank you for having the confidence in me.

My greatest appreciation also goes to Mr Askar Triwiyanto who had given me a tremendous amount of help and there is no way I could ever repay you. I never met someone so helpful like you. I am so happy and glad that I could work with someone so positive and hardworking, someone so inspiring. Truth be told, you inspire me a lot, in so many good ways. You always give me the drive and support throughout this project. You are always there whenever I need help. I really hope I could work with someone like you in the future.

Last but not least, I also want to thank everybody who have involved and help me along this project both directly and indirectly. I really appreciate it. Thank you so much.

TABLE OF CONTENTS

CHAPTER 1: INTRODUCTION	1
1.1 BACKGROUND OF STUDY.....	1
1.2 PROBLEM STATEMENT.....	2
1.3 OBJECTIVES OF THE RESEARCH.....	3
1.4 SCOPE OF STUDY	3
CHAPTER 2: LITERATURE REVIEW	4
2.1 NITRIDING PROCESS AS EROSION RESISTANCE ENHANCEMENT PROCESS.....	4
2.2 SENSITIZATION OF STAINLESS STEEL	5
2.3 GAS NITRIDING IMPROVING STAINLESS STEEL PHYSICAL PROPERTIES.....	6
CHAPTER 3: METHODOLOGY	8
3.1 FLOW OF ACTIVITY.....	8
3.2 MATERIAL.....	8
3.2.1 AISI 316L Austenitic Stainless Steel	9
3.2.2 9.3%Cr Ferritic Steel.....	9
3.3 EXPERIMENT PROCEDURES.....	10
3.3.1 Sample Preparation	10
3.3.2 Gas Nitriding Process.....	11
3.4 CHARACTERIZATION TECHNIQUES.....	12
3.4.1 Microstructure Imaging.....	12
3.4.2 Elemental Composition and Structural Phase	14
3.4.3 Hardness Measurement	15
CHAPTER 4: RESULT AND DISCUSSION	16
4.1 X-RAY DIFFRACTION RESULT	16
4.1.1 XRD result for austenitic stainless steel 316L nitrided at 600°C.....	16
4.1.2 XRD result for 9.3%Cr ferritic steel nitrided at 600°C.....	16
4.1.3 XRD result for 9.3%Cr ferritic steel nitrided at 900°C.....	17
4.1.4 XRD result for austenitic stainless steel 316L nitrided at 900°C.....	17
4.1.5 Comparison between Untreated & Treated Austenitic Stainless Steel	18
4.1.6 Comparison between Treated 9.3%Cr ferritic steel at Different Temperature Nitriding.....	19
4.2 METALLOGRAPHIC RESULT	20
4.3 SEM MICROGRAPH RESULT	21
4.3.1 Surface of Nitrided Stainless Steel.....	21
4.4 CHROMIUM DEPLETION ON SELECTED AREA	23

4.4.1	9.3%Cr ferritic steel after Nitriding at 600 ^o C	23
4.4.2	Austenitic Stainless Steel after Nitriding at 600 °C	25
4.4.3	9.3%Cr ferritic steel after Nitriding at 900 ^o C	27
4.4.4	Austenitic Stainless Steel after Nitriding at 900 ^o C.....	29
4.5	UNIVERSAL SCANNING PROBE MICROSCOPY	30
4.5.1	Surface Topography	30
4.5.2	Surface Phase	31
4.5.3	Surface Roughness	32
4.6	SURFACE MICROHARDNESS.....	35
CHAPTER 5: CONCLUSION AND RECOMMENDATIONS		37
5.1	CONCLUSION	37
5.2	RECOMMENDATION.....	38
REFERENCES.....		39

LIST OF TABLES

Table 1:	Chemical Composition of Austenitic Stainless Steel.....	9
Table 2:	Chemical Composition of 9.3%Cr Ferritic Steel	9
Table 3:	Parameter of nitriding for different temperature.....	11
Table 4:	Parameter of Nitriding	21
Table 5:	Roughness Average.....	32

LIST OF FIGURES

Figure 1: $M_{23}C_6$ on grain boundary.....	6
Figure 2: Diagram shows chromium carbide particles precipitated along grain boundaries in stainless steel	6
Figure 3: Flow of Project	8
Figure 4: Low Speed Precision Cutter	10
Figure 5: Horizontal nitriding furnace	11
Figure 6: Carl Zeiss Optical Microscope	12
Figure 7: (a) Supra 55VP FESEM (b) Nano Navi: E-sweep USPM.....	13
Figure 8: PentaFET Precision EDS	14
Figure 9: D8 Advance XRD machine	15
Figure 10: XRD result nitrided austenitic stainless steel 316L at 600°C	16
Figure 11: XRD result nitrided 9.3 Cr Ferritic Steel at 600°C	16
Figure 12: XRD result nitrided 9.3 Cr Ferritic Steel 316L at 900°C	17
Figure 13: XRD result nitrided austenitic stainless steel 316L at 900°C	17
Figure 14: Comparison between Untreated and Treated Austenitic Stainless Steel ..	18
Figure 15: Nitrided 9.3 Cr Ferritic Steel at Different Temperature	19
Figure 16: Metallographic of material after nitriding process using 40X mag	20
Figure 17: SEM micrograph of the surface of material after nitriding process	21
Figure 18: Elemental mapping for 9.3%Cr ferritic steel after nitriding at 600°C	24
Figure 19: Elemental mapping for austenitic stainless steel after nitriding at 600°C ..	26
Figure 20: Elemental mapping for 9.3%Cr ferritic steel after nitriding at 900°C:....	28
Figure 21: Elemental mapping for austenitic stainless steel after nitriding at 900°C ..	29
Figure 22: Surface topography of material	30
Figure 23: Surface phase of material.....	31
Figure 24: Surface Roughness of Untreated 9.3%Cr ferritic steel	32
Figure 25: Surface Roughness of Nitrided 9.3%Cr ferritic steel at 600°C	33
Figure 26: Surface Roughness of Nitrided 9.3%Cr ferritic steel at 900°C	33
Figure 27: Surface Roughness of Untreated Austenitic Stainless Steel.....	33
Figure 28: Surface Roughness of Nitrided 9.3%Cr ferritic steel at 600°C	34
Figure 29: Surface Roughness of Nitrided Austenitic Stainless Steel at 900°C	34
Figure 30: Depth profile of microhardness	35

ABBREVIATIONS

fcc	face centred cubic
bcc	body centred cubic
$M_{23}C_6$	Chromium Carbides
CE	Cavitations Erosion
PVD	Physical Vapour Deposition
CVD	Chemical Vapour Deposition
H	Hydrogen
N_2	Nitrogen gas
NH_3	Ammonia
FESEM	Field Emission Scanning Electron Microscope
USPM	Universal Scanning Probe Microscope Machine
AFM	Atomic Force Microscope
EDS	Energy Dispersive X-ray Spectroscopy
XRD	X-ray Diffraction
Cr	Chromium
Ra	Roughness Average

CHAPTER 1: INTRODUCTION

1.1 BACKGROUND OF STUDY

The austenitic stainless steel consist primarily of single phase, face-centred cubic (fcc) austenite and non-magnetic. The structure of austenitic stainless steel characterized by relatively low yield strength, high work hardening rate and high tensile strength. Beside that, this type of stainless steel has good ductility and formability, especially good low temperature toughness and inability to be hardened by heat treatments process [1, 2]. However, high performance stainless steel as 316L is easily form second phases at high temperatures. These phases will damage certain corrosion resistance and mechanical properties of the steel. Therefore, the application for austenitic stainless steel at high temperature is limited. Austenitic has been used for food preparation equipment particularly in chloride environment, pharmaceutical, marine application, architectural application, medical implant and fastener [3].

There are many types and grade of steel. Ferritic steels are chromium containing alloys with body centred cubic (bcc) crystal structures. Chromium content is typically less than 30%. The ferritic steels are ferromagnetic. They may have good ductility and formability, but high-temperature mechanical properties are relatively inferior to the austenitic stainless steels. Toughness is limited at low temperatures and in heavy sections. Ferritic steel is used because the ferritic structure has unique attribute of being high oxidation and corrosion resistance. However, at high temperature the steel strength and toughness is poor. Ferritic steel is a candidate material in less severe corrosion atmosphere for chemical processing equipment, furnace parts, heat exchangers, petroleum refining equipment, recuperators, storage vessels, electrical appliances, solar water heaters, and household appliances [4]. Despite these economic and metallurgical attributes, the ferritic steels are less used in engineering application. This is because the ferritic steels are prone to intergranular corrosion attack at certain temperature zone.

In order to achieve the good physical and metallurgical characteristic, 9.3%Cr ferritic steel and austenitic stainless steel need to be undergone surface hardening process. Beside of the various surface hardening technique available [5, 6], nitriding offers benefits in term of high dimensional stability. At high temperature, the gas nitriding technique for nitriding of high alloyed had increased degree of hardness of nitrated layer but worsening the corrosion resistance. This is called sensitization which associated with chromium carbides, $M_{23}C_6$ along grain boundaries during the heat treatment [7]. Therefore, studies need to be done at critical chromium depletion zone to clarify and verify this matter.

1.2 PROBLEM STATEMENT

Sensitization is a detrimental process which can occur in stainless steels including austenitic stainless steel and 9.3%Cr ferrite steel. Sensitization is where the chromium depletion occurs that can reduce the alloy's corrosion resistance from the expected value. Knowledge of the interrelationships of the major and minor alloying elements would permit an evaluation of the effect of an added impurity on grain boundary chemistry and subsequent intergranular corrosion and stress corrosion cracking. Since only minimum chromium content is required to maintain the passive film necessary for resistance to electrochemical attack, the result of chromium depletion is that the steel becomes sensitized to possible intergranular corrosion. The chromium carbide precipitates along grain boundary of the alloy during the heat treatment [1, 8].

The gas nitriding process which will improve the properties and characteristic of the stainless steel significantly is the heat treatment that the researcher will used in this research. The chromium and carbon must disseminate to the grain boundaries to form the percipitates, which leaves a chromium depleted zone adjacent to the grain boundary. Research from Demo et al [9] had found out that precipitation at the range of 500°C to 800°C will resulting sensitization leading to intergranular corrosive environment. Therefore, this research focuses on the chromium depletion occurrence for austenitic stainless steel and 9.3%Cr steel at the temperature of 600°C and 900°C after the nitriding treatment. This is to ensure that at these temperatures which is

close at chromium depletion zone, the chromium carbides, $M_{23}C_6$ could be possibly occur along grain boundary at these temperature zone.

1.3 OBJECTIVES OF THE RESEARCH

The aim of this research is to study the possibilities of using austenitic stainless steel and 9.3%Cr ferritic steel at temperature of 600°C and 900°C which is close to theoretical of sensitization known as the critical temperature zone of chromium depletion formation. The physical and mechanical properties of nitrided austenitic stainless steel and 9.3% Cr steel also being studied in this research

1.4 SCOPE OF STUDY

The study focus on the chromium carbides, $M_{23}C_6$ presence at grain boundary region of austenitic stainless steel and 9.3%Cr ferritic steel at temperature of 600°C and 900°C. The mechanical and physical properties of the 316L austenitic stainless steel and 9.3%Cr steel after gas nitriding process also being studied. The 316L austenitic stainless steel and 9.3%Cr ferritic will be nitrided using gas nitriding process in the furnace. There are two different parameters that used for nitriding process. The scope of the work is to perform nitriding at different period of nitrogen diffusion. Then, the nitrided samples will be analysed in term of physical and mechanical properties. The samples will be tested by various testing such as optical test, x-ray diffraction, field emission scanning electron machine, hardness test and magnetic test. These tests are done to investigate the difference of properties between untreated ferritic stainless steel samples and nitrided samples. By comparing the treated samples and controlled sample, the researcher can determine either sensitization had occurred on the nitrided sample or not.

CHAPTER 2: LITERATURE REVIEW

2.1 NITRIDING PROCESS AS EROSION RESISTANCE ENHANCEMENT PROCESS

Based on the previous research, the heat treatment process had proven as a technique to increased cavitations erosion resistance of the stainless steel. As the gas nitriding is one of heat treatment technique, the cavitations erosion of the stainless steel will increase after undergone this process [10]. Berns et al. showed that when heat treatment gas nitriding is applied to austenitic–ferritic, martensitic and austenitic stainless steels, their cavitations erosion (CE) resistance is considerably increased

The improvement in CE resistance was attributed to the increase in planar dislocation slip and to an increase in metallic characteristics of the interatomic bonding (due to an increase in the concentration of free electrons), leading to a particularly high combination of toughness and yield strength [11]. Dos Santos et al. showed that, in an UNS S30403 austenitic SS, the increase in the nitrogen content up to 0.48 wt% in solid solution increases the incubation time (4.5 times) and decreases the wear rate (8.5 times).

Tschiptschin and Toro [12] reported that the increasing resistance to plastic flow is one of the key features controlling the performance of high nitrogen austenitic stainless steels during CE.

2.2 SENSITIZATION OF STAINLESS STEEL

Sensitization refers to decrease of corrosion resistance when stainless steel being cooled down from annealed temperature or undergo high temperature heating process. Currently, the chromium depletion theory is generally accepted as main reason for sensitization problem. Sensitization is a common problem in austenitic steel where precipitation of chromium carbides (Cr_{23}C_6) occurs at the grain boundaries at elevated temperatures. Several experimental studies have shown the correlation of the onset of sensitization with presence of carbides at grain boundary.

According to previous research done by Z.L. Zhang and T. Bell. Surf, temperatures in excess of 480 °C during nitriding in stainless steel cause precipitation of chromium nitride and chromium carbide. The precipitate will cause intergranular corrosion along the grain boundary in stainless steel during the gas nitriding. Beside, the chromium depletion along the grain boundary will lead to low material strength as it can start the internal cracking in the stainless steel.

Qualitative method had been developed to study on sensitization phenomena. Originally, the model has been proposed by Bain et al [13] where his research team had found out that the chromium content is reduced in regions adjacent to precipitating chromium carbide. When chromium level falls below that required for passivation, the material become prone to sensitization. Strawstorm and Hillert [14] had developed a model based chromium diffusion control to calculate time to sensitization. In their research, they had calculated the chromium content at carbide interface by considering the changing equilibrium during precipitation of M_{23}C_6 in austenitic in Fe-Cr-Ni alloys.

The precipitation of M_{23}C_6 has been the focus of many investigations, motivated by its importance in terms of corrosion resistance. M_{23}C_6 on grain boundaries is often associated with intergranular corrosion. It is found after very short ageing times (30 mn at 750 °C, Lewis *et al.*, [15]), even in stabilised steels. It causes the grain boundary to move, and therefore shows on one side, the new grain boundary. These precipitates are usually large. When boron is added, the number density of M_{23}C_6 along the grain boundaries increases (Tanaka *et al.*, 1997, [16]),

with beneficial effect for the creep rupture strength, as the grain boundary sliding and surface cracking are reduced.

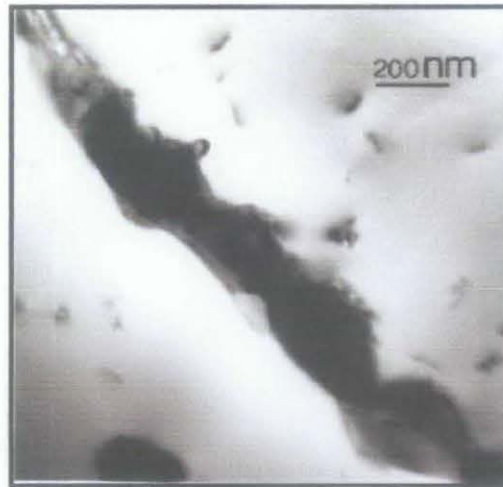


Figure 1: $M_{23}C_6$ on grain boundary.

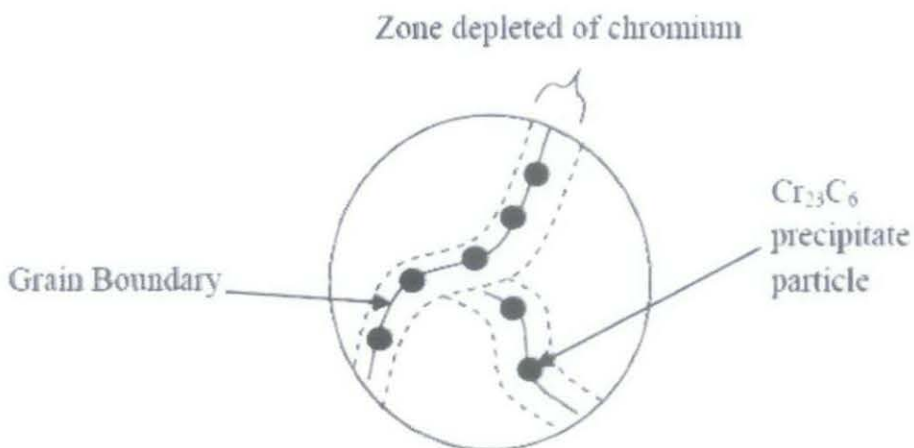


Figure 2: Diagram shows chromium carbide particles precipitated along grain boundaries in stainless steel [17]

2.3 GAS NITRIDING IMPROVING STAINLESS STEEL PHYSICAL PROPERTIES

Surface engineering consists of all scientific and technical problems that are related to the production of surface layers prior to post-use or service or during service, on or under the surface or on a substrate, with properties which vary from materials that may be introduced to the exterior of the core in the state of solid, liquid and gas. It also takes into account research of related phenomena and of potential and usable properties of surface layers, including problems connected with layer design.

Several types of surface engineering have been proposed to pull off the desired surface properties. Fundamentally, there are two distinguished methods used: which are depositional techniques and diffusional techniques. Depositional techniques are characterised as transporting a substance from derivative sources and depositing it onto the surface of the treated materials, and include electroplating, physical vapour deposition (PVD), and chemical vapour deposition (CVD). As for stainless steels, these materials have a good mixture of strength and corrosion resistance, but they lack in the wear resistance. There are established processes to increase hardness. According to V. Muthukumaran et al, [18], the layer can had higher hardness value than untreated sample and keeps good corrosion resistance. To obtain treatment depths of several tens of micrometers in a reasonable time, these processes operate at elevated temperatures required.

Through diffusional techniques in surface hardening processes include carburizing, nitriding, carbonitriding, and nitrocarburizing. These methods change the chemical composition of the steel, carburizing by adding carbon, nitriding through the addition of nitrogen and nitrocarburizing by the adding both nitrogen and carbon into the combination. Conventionally, the method mentioned in hardening the surface have been performed by metallurgists for many years using gaseous and salt bath processes . However, more efficient and environmental friendly surface treatment such as controlled gas treatment, ion plantation and plasma nitriding are now commercially available in improving the surface properties.

CHAPTER 3: METHODOLOGY

3.1 FLOW OF ACTIVITY: The activity flow is shown in Figure 3.

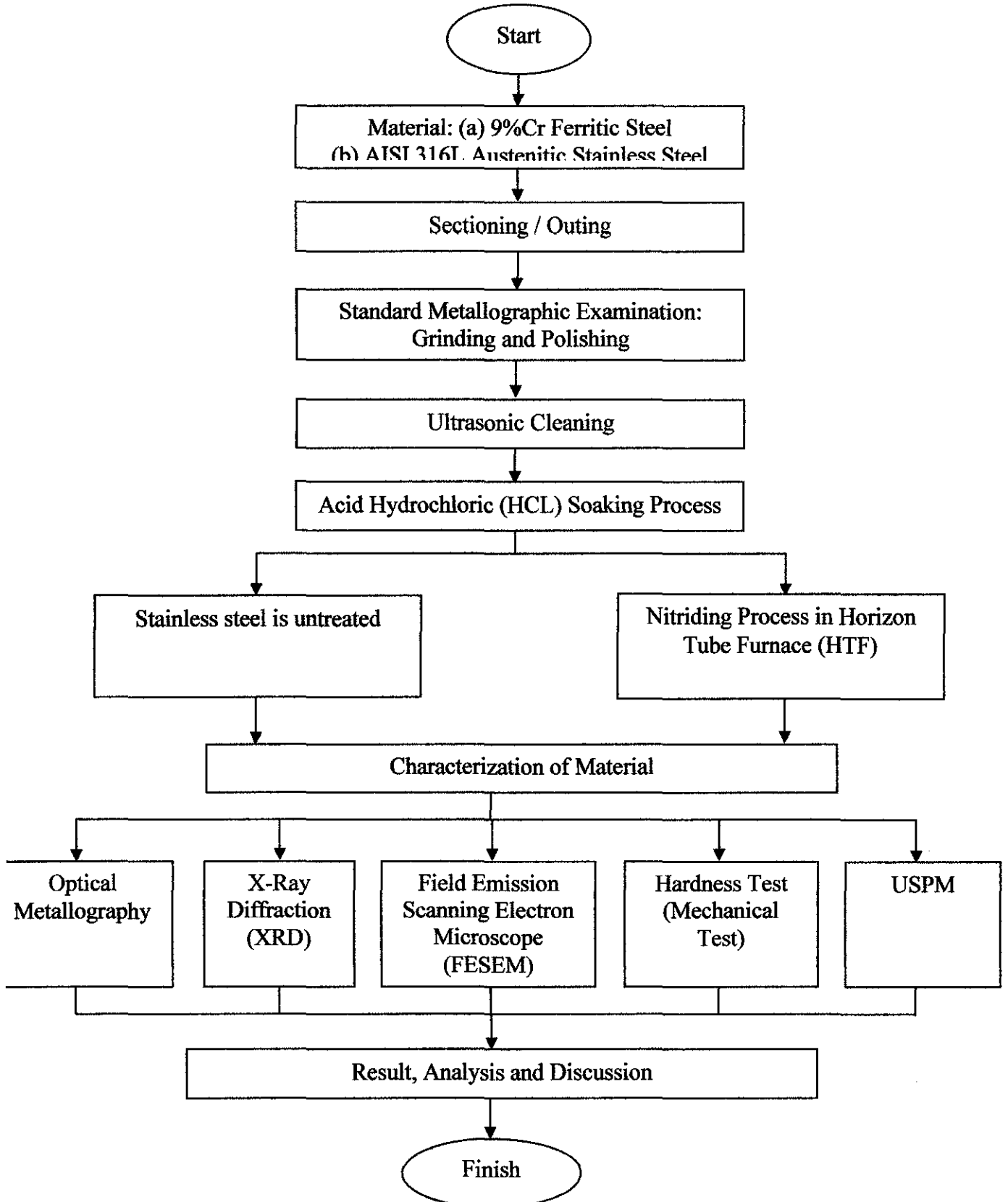


Figure 3: Flow of Project

3.2 MATERIAL

3.2.1 AISI 316L Austenitic Stainless Steel

The dimension of austenitic stainless steel supplied is 16mm diameter in form of round bar. The chemical composition of this material is as in Table 1.

Table 1: Chemical Composition of Austenitic Stainless Steel

Chemical Composition	Percentage
Carbon, C	0.02%
Chromium, Cr	17.19%
Chromium, Co	0.31%
Nickel, Ni	11.54%
Phosphorus, P	0.03%
Silicon, Si	0.42%
Manganese, Mn	1.7%
Molybdenum, Mo	2.06%
Sulphur, S	0.002%
Iron, Fe	Balance

3.2.2 9.3%Cr Ferritic Steel

The dimension of 9.3%Cr ferritic steel supplied is 16mm diameter in form of round bar. The chemical composition of this material is as in Table 2.

Table 2: Chemical Composition of 9.3%Cr Ferritic Steel

Chemical Composition	Percentage
Carbon, C	0.016%
Chromium, Cr	9.3%
Molybdenum, Mo	0.61%
Nickel, Ni	0.95%
Sulphur, S	0.002%
Silicon, Si	0.35%
Manganese, Mn	0.68%
Vanadium, V	0.29%
Iron, Fe	87.8%

3.3 EXPERIMENT PROCEDURES

3.3.1 Sample Preparation

3.3.1.1 Sectioning / Outing

The samples were cut with appropriate thickness using low speed precision cutter machine (Figure 4). The thickness used in this experiment is 2mm. There were 4 samples were prepared for this experiment.



Figure 4: Low Speed Precision Cutter

3.3.1.2 Standard Metallographic Examination: Grinding and Polishing

The samples were ground and polished before nitriding process could be carried out. This process to ensure that only polishing was required to produce a good surface finish after the nitriding process in order to avoid removing too much nitrated layer on the material.

3.3.1.3 Ultrasonic Cleaning and Hydrochloric Acid Soaking

Samples were washed with methanol or acetone before nitriding process was carried out. The process was carried out using ultrasonic cleaning method. Then, the samples had been soaked with hydrochloric acid. 4 samples were used for nitriding process while the other two will be used as comparison.

3.3.2 Gas Nitriding Process

3.3.2.1 Parameter of Nitriding

The parameter used for nitriding process is shown as in Table 3.

Table 3: Parameter of nitriding for different temperature

Temperature = 600 °C	Temperature = 900 °C
NH ₃ flow rate : 250 cm ³ /min	NH ₃ flow rate : 250 cm ³ /min
H ₂ flow rate : 150 cm ³ /min	N ₂ flow rate : 250 cm ³ /min
Time : 2 hours	Time : 8 hours

3.3.2.2 Nitriding Process Procedure

Samples were placed in the boat. Then, the sample were inserted in the cold zone while the air in the furnace was being purged with nitrogen for at least 15 minutes at a flow rate of 200cm³/min in order to prevent oxidation of the samples. The boat was carefully pushed into the hot zone of the furnace where nitriding was takes place after purging process. Samples were treated with various gases, temperatures, length of time and gas flow rates. Nitriding was carried out at temperatures of 600°C in a gas mixture of 100cm³min⁻¹ of H₂ and 250cm³min⁻¹ of NH₃ for the first sample for 2 hours. The second sample was nitrided at 900°C in a gas mixture of 500cm³min⁻¹ of N₂ and 500cm³min⁻¹ of NH₃ for variables 8 hours. After nitriding for the specified time, samples were removed from the furnace and immediately cooled in air to the room temperature. The horizontal nitriding furnace that was used is shown in Figure 5.



Figure 5: Horizontal nitriding furnace

3.4 CHARACTERIZATION TECHNIQUES

Quantitative and qualitative characterisation of the microstructural, elemental composition, structural phase and mechanical properties of the samples were examined using several of instruments.

3.4.1 Microstructure Imaging

3.4.1.1 Optical Metallography

Specimens for optical microscopical studied were either mounted in bakelite or were set in cold setting epoxy resin. These specimens were abraded through various grades of silicon carbide paper down to 1200 grit. Then, the specimens were polished to 1 μ m diamond finish using blue lubricant. The etchant used was 6g cupric chloride, 100mls methanol, 100mls distilled water and 100mls concentrated hydrochloric acid. Carl Zeiss Optical Microscope (Figure 6) was used to study microscopical of the specimens.



Figure 6: Carl Zeiss Optical Microscope

3.4.1.2 Field Emission Scanning Electron Microscope (FESEM)

A SUPRA 55VP FESEM (Figure 7 (a)) was used to study the precipitation of phases. FESEM with ultra high-resolution imaging is designed to fulfil the requirements of analysing up to nano scale surface and morphology of the stainless steel. A well-defined electron beam impinges on the specimen and leads to generation of secondary electron, back scattered electrons, absorbed

electron and characteristic X-ray. These electrons can be detected by suitable detectors and give information about surface structure as well as morphology of the stainless steel. X-ray Energy Dispersive Analysis was used to determine the chemical composition of the phases as well as the elemental diffusion from the sialon to stainless steel.

3.4.1.3 Universal Scanning Probe Microscope (USPM)

USPM is the general term used to describe a microscope that allows the high magnification observation of 3D topographic images, force modulation images, magnetic images, friction images and electric-potential images by scanning a sample surface with a microscope probe. USPM also be used in order to inspect on the sub-nanometer scale which in this research the surface topography of treated and untreated specimens from top-view were explored. Atomic force microscope (AFM) is another type of USPM which had been widely used for surface characterization. The simple tip used in AFM is attached to the end of cantilever with 100 to 200 μm long. The main data measured is the deflection of laser beam on the cantilever when force between tip and the surface bend the cantilever. In this research, surface topography, surface phase and surface roughness was characterized by AFM in contact mode on the treated sample and untreated samples using USPM shown in Figure 7 (b).

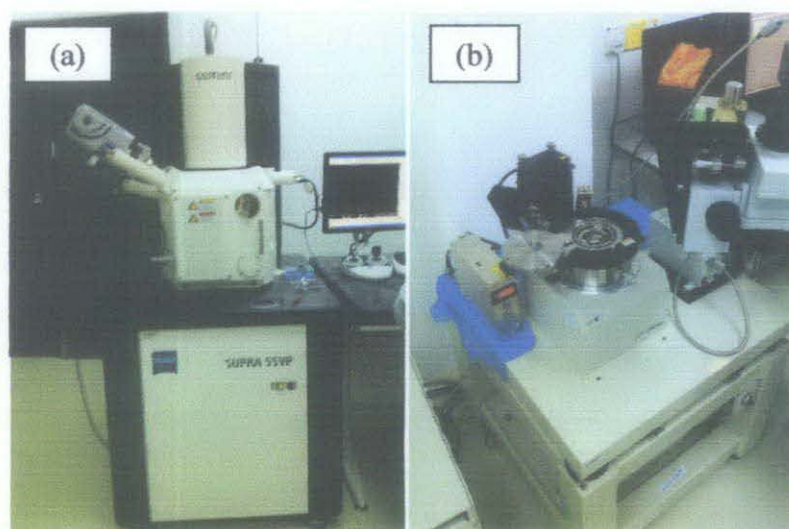


Figure 7: (a) Supra 55VP FESEM (b) Nano Navi: E-sweep USPM

3.4.2 Elemental Composition and Structural Phase

3.4.2.1 Energy Dispersive X-ray Spectroscopy (EDS)

Energy dispersive x-ray spectroscopy was used in FESEM to gather the elemental composition data on treated layers of material. The relative proportions of the elements present in the sample were determined from the relative signal intensities detected. However, it should be noted that there is an inherent inaccuracy using EDS for quantitative analysis of samples containing oxygen. Atomic percent values are generally only accurate to within 10%. The size of electron probe volume was roughly calculated using a Monte Carlo simulation. The electron penetration depth determined for 15kV accelerating voltage used was found to be $1\mu\text{m}$. EDS was conducted on the hardened layer in section, which gave information of the composition of bulk of the layers without interference of substrate alloy. Areas in the middle of the sample were selected in random, well away from outer or inner edges of the coating. Multiple locations on the surface of the layers were also investigated to determine the relation of the surface composition to bulk composition of the treated layers. In this research, the elemental compositions of the treated samples were obtained using FESEM equipped with PentaFET Precision EDS (Figure 8).



Figure 8: PentaFET Precision EDS

3.4.2.2 X-ray Diffraction (XRD)

Powder diffraction techniques have a wide variety of applications in compositional, structural, microstructural and many other areas. The broadening of reflections in a powder diffraction pattern contains much information, such as crystallite strain, shape and stacking faults [19]. Characterisation of solid and powder samples was carried out in a powder diffraction using monochromated $\text{CuK}\alpha$ radiation. A step scanning motor was used and controlled by a microcomputer which also recorded the data. The XRD analysis was done using D8 Advance XRD machine as shown in Figure 9.



Figure 9: D8 Advance XRD machine

3.4.3 Hardness Measurement

3.4.3.1 Surface Microhardness

Hardness measurements were carried out on metallographic specimens using a microhardness apparatus with 10g load. The machine that was used to perform the hardness test was micro hardness tester Model LECO LM247 AT. The purpose of this test is to observe the questioned materials' ability to resist plastic deformation from a standard source. Hardness values were read using an x40 magnifier and converted to Vickers-hardness using tables.

CHAPTER 4: RESULT AND DISCUSSION

4.1 X-RAY DIFFRACTION RESULT

The actual parameters of nitriding process used for duration of 2 hours are as follows:

- NH_3 flow rate : $250 \text{ cm}^3/\text{min}$
- H_2 flow rate : $150 \text{ cm}^3/\text{min}$

4.1.1 Figure 10 shows the XRD result for austenitic stainless steel 316L nitrided at 600°C .

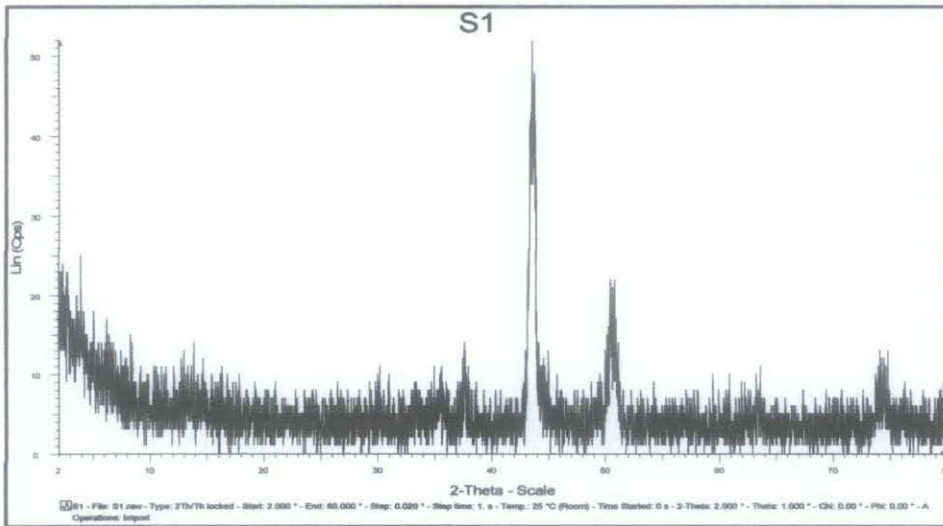


Figure 10: XRD result nitrided austenitic stainless steel 316L at 600°C

4.1.2 Figure 11 shows the XRD result for 9.3%Cr ferritic steel nitrided at 600°C .

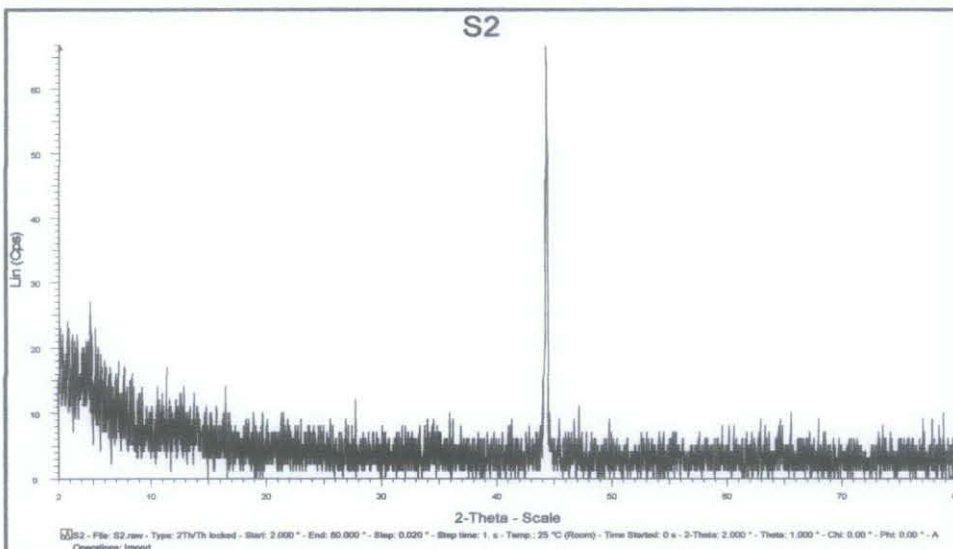


Figure 11: XRD result nitrided 9.3 Cr Ferritic Steel at 600°C

The actual parameters of nitriding process used for duration of 8 hours are as follow:

- NH_3 flow rate : $250 \text{ cm}^3/\text{min}$
- N_2 flow rate : $250 \text{ cm}^3/\text{min}$

4.1.3 Figure 12 shows the XRD result for 9.3%Cr ferritic steel nitrided at 900°C .

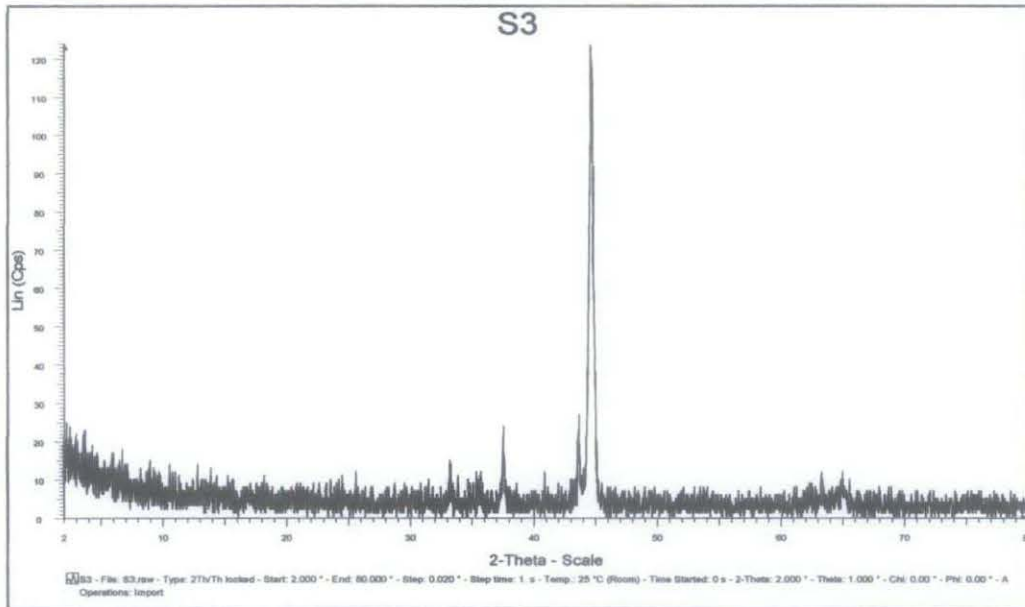


Figure 12: XRD result nitrided 9.3 Cr Ferritic Steel 316L at 900°C

4.1.4 Figure 13 shows the XRD result for austenitic stainless steel 316L nitrided at 900°C .

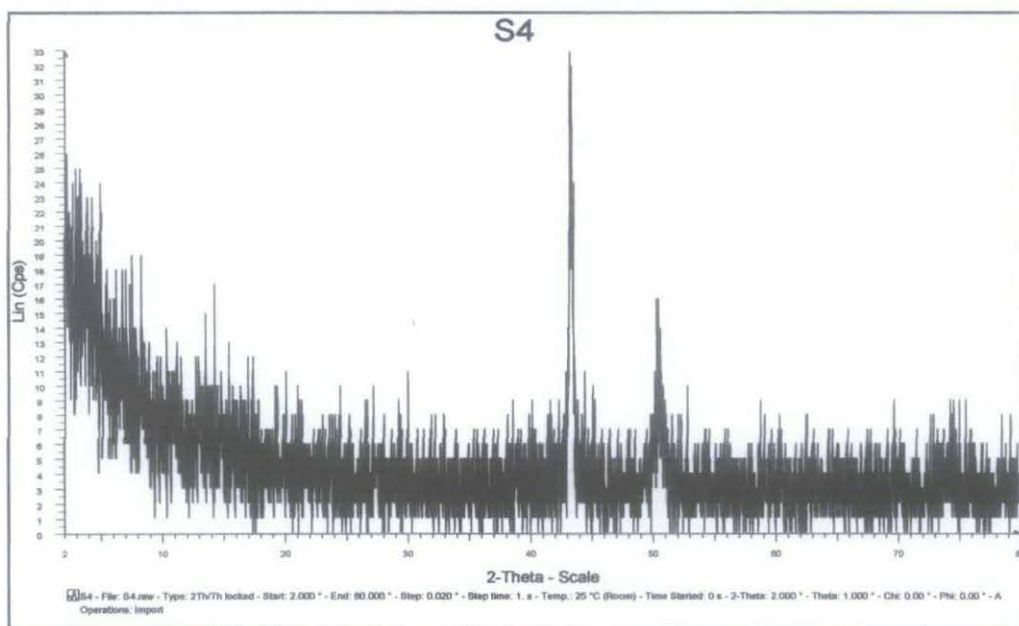


Figure 13: XRD result nitrided austenitic stainless steel 316L at 900°C

4.1.5 Comparison between Untreated and Treated Austenitic Stainless Steel

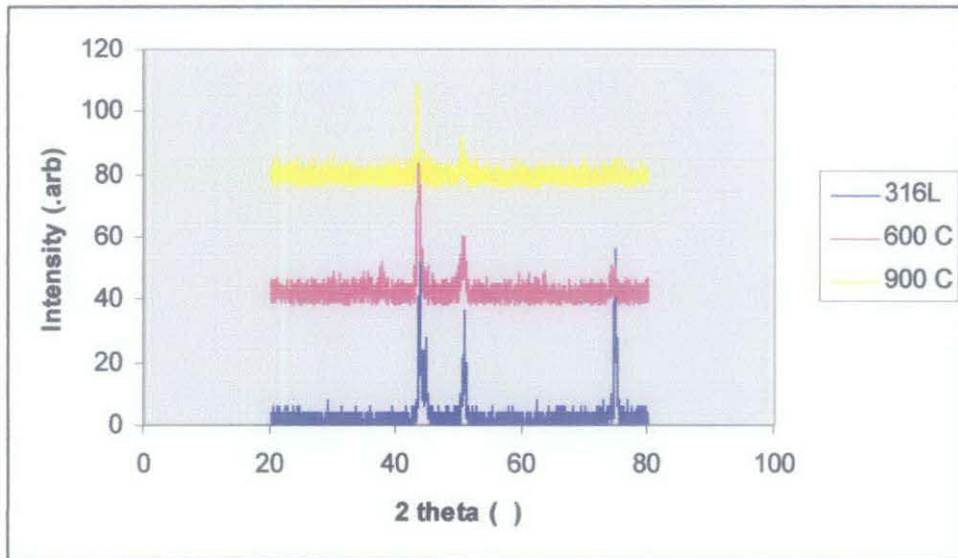


Figure 14: Comparison between Untreated and Treated Austenitic Stainless Steel

XRD analyses were performed using a Bruker D8 Advanced diffractometer instrument equipped with a CuK α radiation source, operated at 40 kV and 30 mA. The XRD pattern of untreated/as received specimen and other specimen (nitrided 600 °C and 900 °C) with different parameters as shown in Figure 14. The untreated specimen consists of mainly fcc- γ (austenite). Distinctive phases of the treated specimens are CrN resulting from high temperature treatment parameters which indicates that nitriding at 600 °C and 900 °C caused the formation of CrN precipitates leading to the sensitivity effect of the material.

As can be seen in the Figure 14, the significant amount of nitrogen dissolved in the layer obviously leads to the supersaturation of the austenite lattices. The austenite lattice in the surface alloyed layer is expanded as evidenced from the small shift of the XRD peaks to lower diffraction angles as compared to the corresponding peaks from the untreated substrate. According to the XRD results, a lattice expansion by 0.4% was found for the CrN phase in this study. These lattice expansions were calculated from XRD peak shift which was developed by previous study [20]. In this investigation, however, a calculation of lattice expansion correlated to nitrogen content was not performed because of the lack of quantification of N concentration by EDS.

4.1.6 Comparison between Treated 9.3%Cr ferritic steel at Different Temperature Nitriding

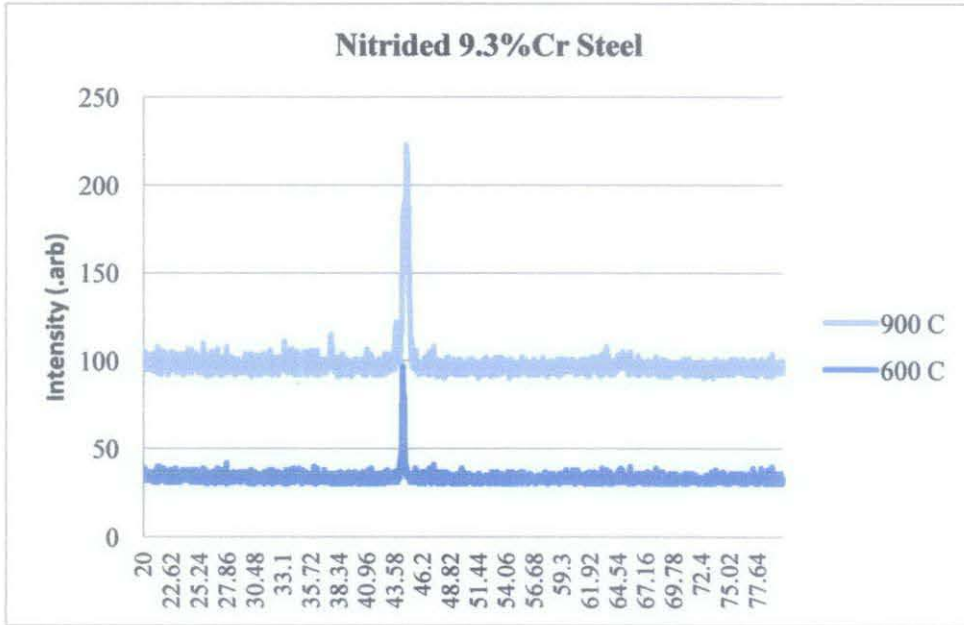


Figure 15: Nitrided 9.3 Cr Ferritic Steel at Different Temperature

Same phenomena also occur for nitrided 9.3%Cr ferritic steel. Distinctive phases of the treated specimens are CrN resulting from high temperature treatment parameters which indicates that nitriding at 600 °C and 900 °C caused the formation of CrN precipitates leading to the sensitivity effect of the material. The treatment at 900°C show significant shift compared to nitriding process at 600°C which mean the ferritic steel nitrided at 900°C more sensitized as shown in Figure 15.

4.2 METALLOGRAPHIC RESULT

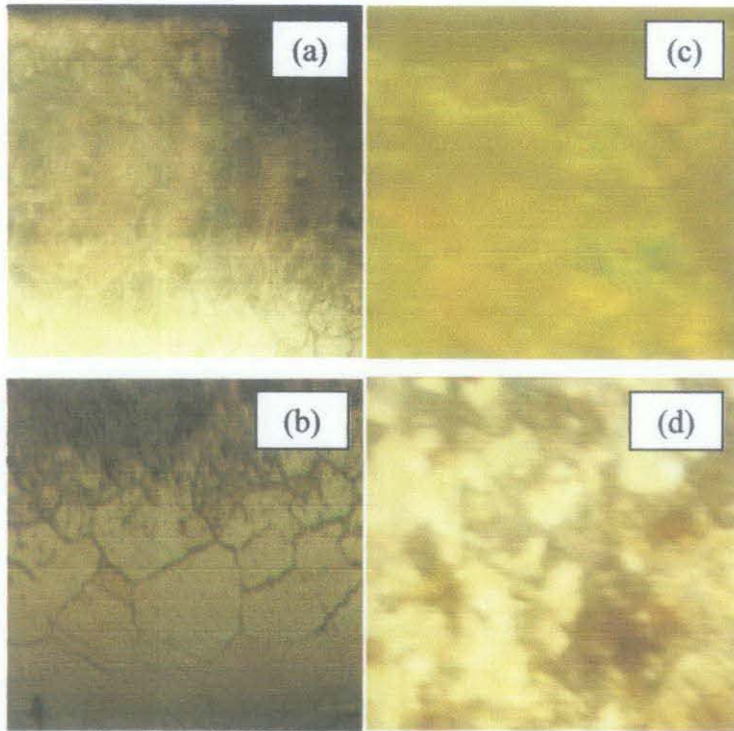


Figure 16: Metallographic of material after nitriding process using 40X magnification: (a-b) austenitic stainless steel and (c-d) 9.3%Cr ferritic steel

Figure 16 shows the optical micrographs of 316L stainless steel and 9.3%Cr ferritic steel which had been (a) nitrided at 600°C (b) 900°C (c) 600°C and (d) 900°C. The steel shown in the figures had undergone nitriding process successfully since the hardening layer is present in each of the specimens. The hardening layer thickness is different depending on type of material and nitriding temperature. For austenitic stainless steel, the hardening layer much thicker after nitriding process at temperature of 900°C (Figure 16 (b)) compared to austenitic stainless steel that had been nitrided at 600°C (Figure 16 (a)). Contrary with characteristic of austenitic stainless steel, the 9.3%Cr ferritic steel had thicker hardning layer after being nitrided at 600°C (Figure 16 (c)) rather than nitrided sample at 600°C (Figure 16 (d)). In addition, the sizes of the microstructure slightly increase by extending the nitriding temperature range from 600°C to 900°C.

4.3 SEM MICROGRAPH RESULT

4.3.1 Surface of Nitrided Stainless Steel

The actual 4 setting had been set to produce 4 different samples. The parameters are shown in Table 4.

Table 4: Parameter of Nitriding

Sample	Temperature	Time	NH ₃ flow rate	H ₂ flow rate	N ₂ flow rate
(a)	600 ⁰ C	2 hours	250 cm ³ /min	150 cm ³ /min	0 cm ³ /min
(b)	900 ⁰ C	8 hours	250 cm ³ /min	0 cm ³ /min	250 cm ³ /min
(c)	600 ⁰ C	2 hours	250 cm ³ /min	150 cm ³ /min	0 cm ³ /min
(d)	900 ⁰ C	8 hours	250 cm ³ /min	0 cm ³ /min	250 cm ³ /min

Figure 17 (a - d) shows the SEM images produced based on the setting shown in Table 4.

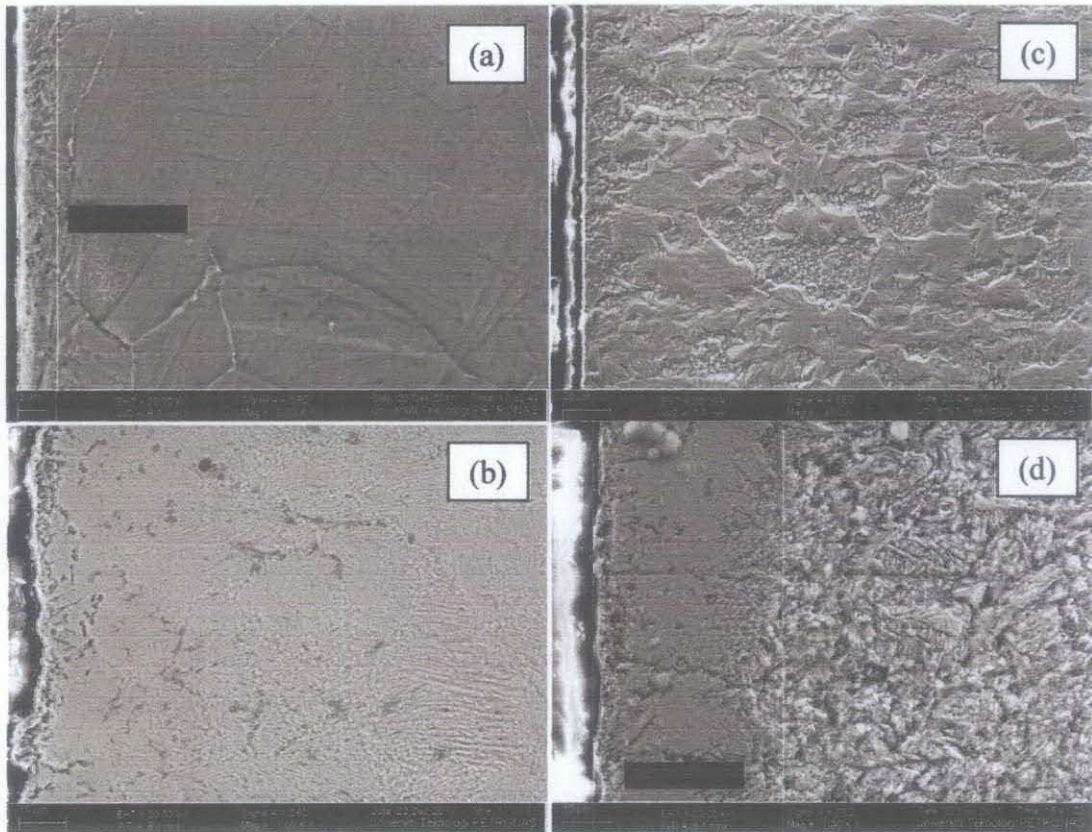


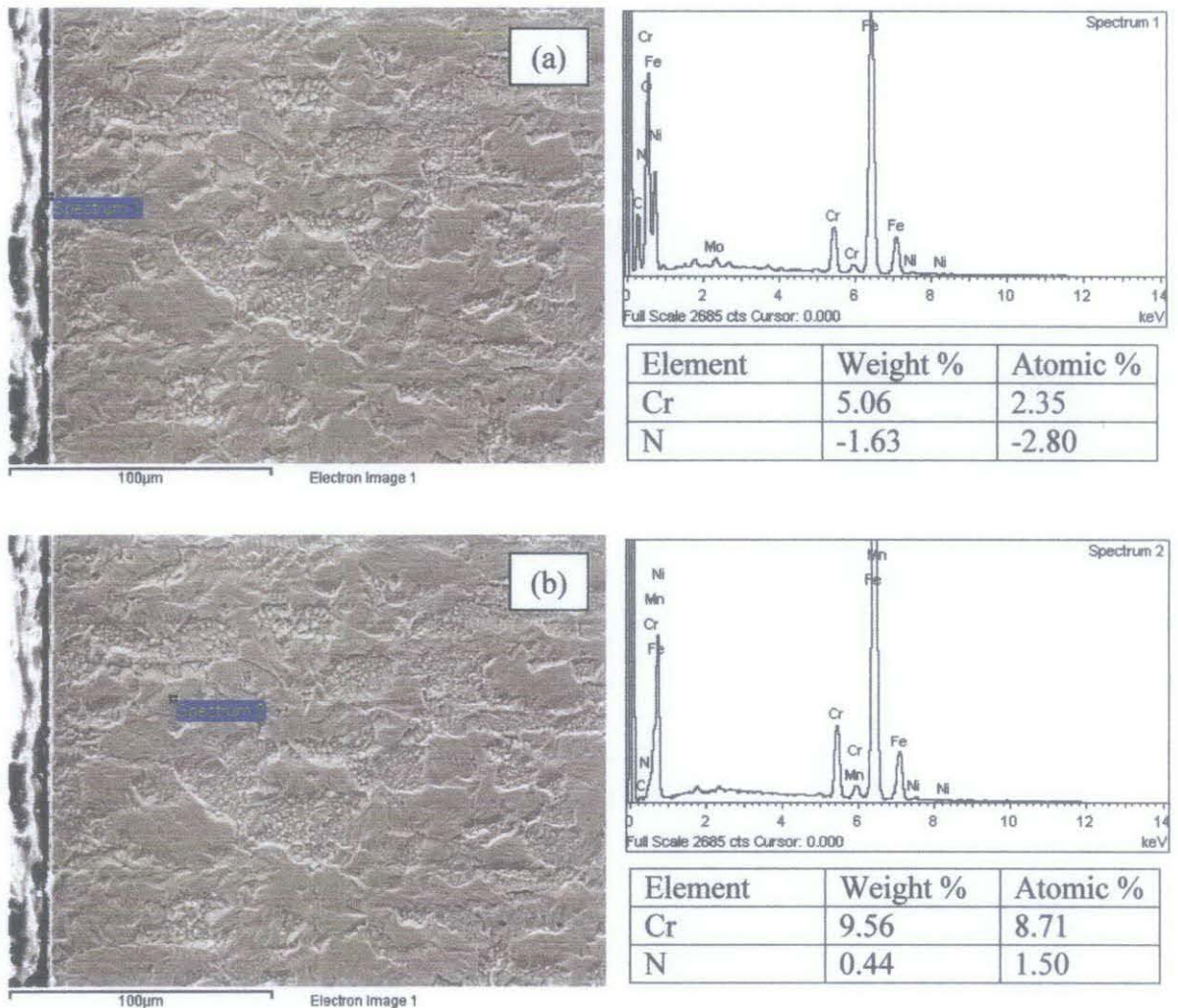
Figure 17: SEM micrograph of the surface of material after nitriding process: (a-b) 316L austenitic stainless steel and (c-d) 9.3%Cr ferritic steel

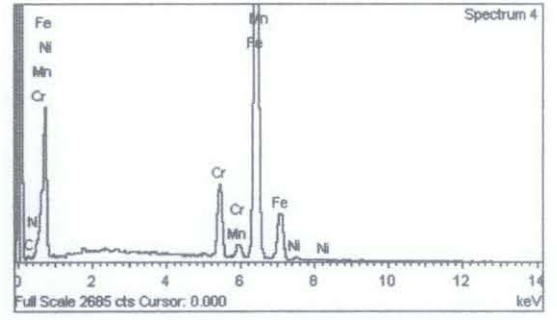
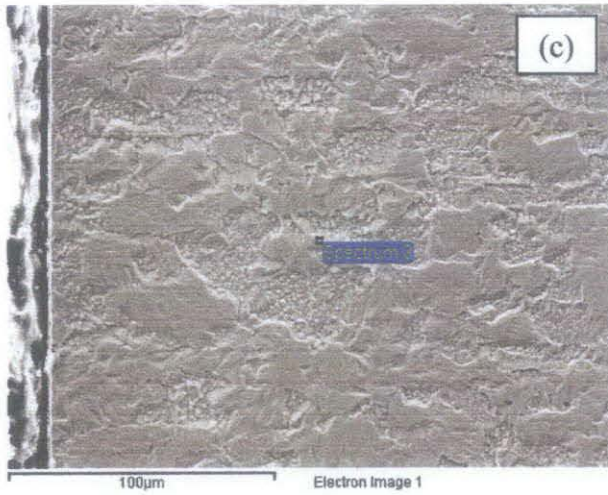
The hardened layer was revealed under SEM micrograph after Marble's etching (4gr CuSO_4 +20ml HCL+20ml H_2O). The hardened layers with different morphologies were observed as a result of various treatment conditions. Figure 17 shows that hardened layer had been produced at different temperature for austenitic stainless steel and 9.3%Cr ferritic steel. During nitriding process at temperature of 600°C for austenitic (Figure 17 (a)), there hardened layer had been produced in low thickness layer. However, the hardened layer can be clearly seen through FESEM analysis on austenitic stainless steel after nitriding process at 900°C . The 9.3%Cr ferritic steel had produced hardened layer after nitriding process at 600°C . There is highest amount of hardened layer produced after process of nitriding at 900°C . From this SEM micrograph analysis, we can conclude that the austenitic stainless steel and 9.3%Cr ferritic steel had changed the characteristic after nitriding process.

4.4 CHROMIUM DEPLETION ON SELECTED AREA

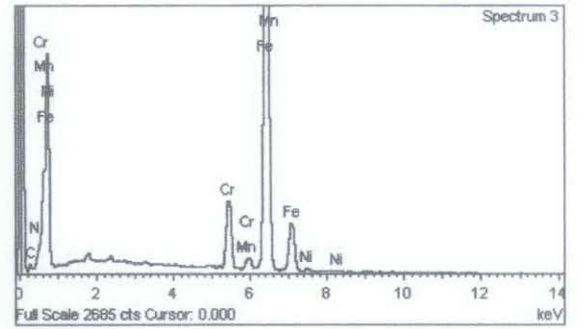
4.4.1 9.3%Cr ferritic steel after Nitriding at 600°C

According to the Figure 18 (a - d), it is shown that at different spots, chromium and nitrogen compositions are fluctuate. At the surface of material, the chromium content is relatively low. The chromium composition started to increase at spectrum 2 (shown in Figure 18 (b)) and suddenly drop as the depth increase (shown in Figure 18 (d)). Then, the chromium content is at high level (Figure 18 (d)) which is at the highest depth. The nitrogen content is increasing as the depth increased showing that the nitriding process had been successfully done.





Element	Weight %	Atomic %
Cr	9.04	7.86
N	0.82	2.65

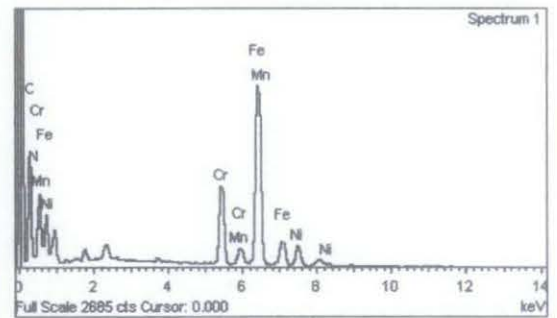
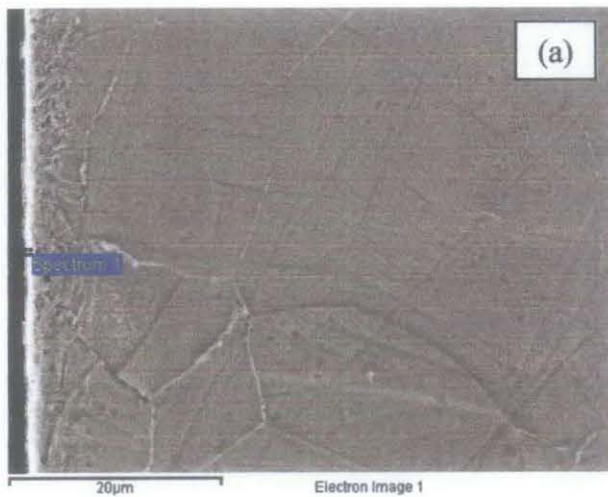


Element	Weight %	Atomic %
Cr	9.55	8.79
N	1.00	3.42

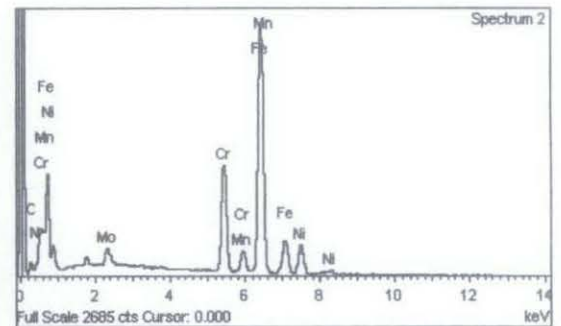
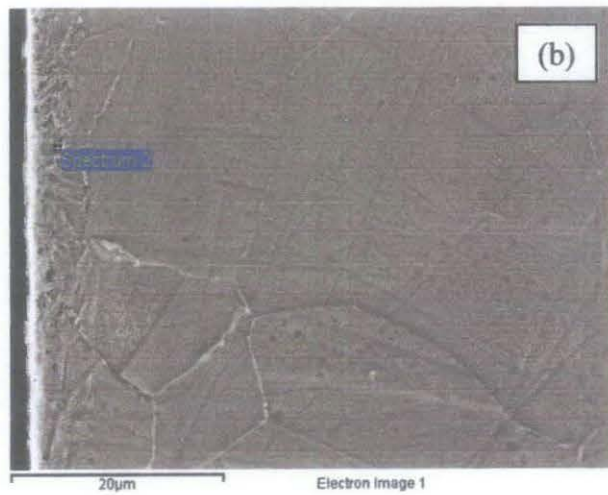
Figure 18: Elemental mapping for 9.3%Cr ferritic steel after nitriding at 600°C: (a) spectrum 1 (b) spectrum 2 (c) spectrum 3 (d) spectrum 4

4.4.2 Austenitic Stainless Steel after Nitriding at 600 °C

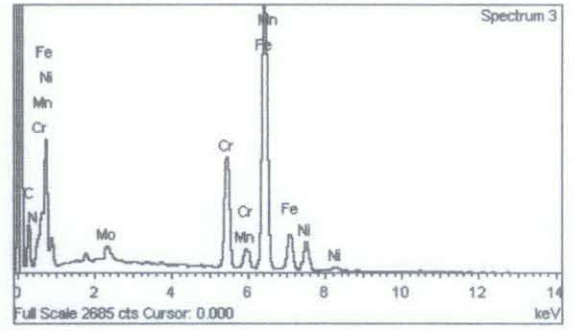
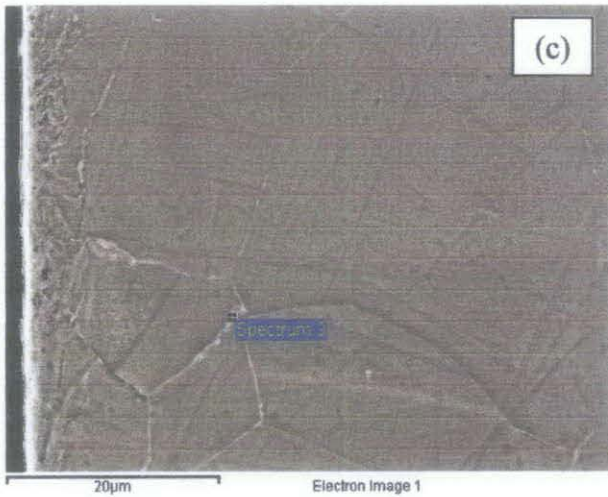
As a result for of nitriding process for austenitic stainless steel at 600°C, the highest chromium content is the area near surface but only small amount at surface is present. At the grain boundary (figure 19 (c)), the chromium is increase as well as in its matrix (figure 19 (d)). The nitrogen behaviour tends to decrease along the depth (Figure 19 (b-d)).



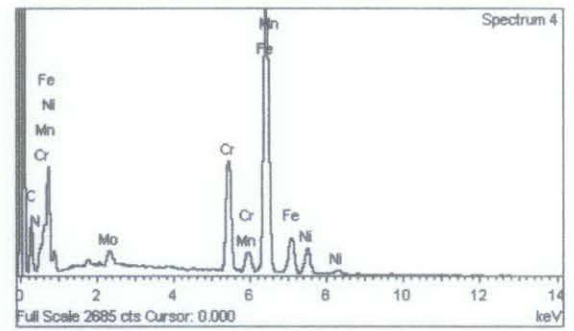
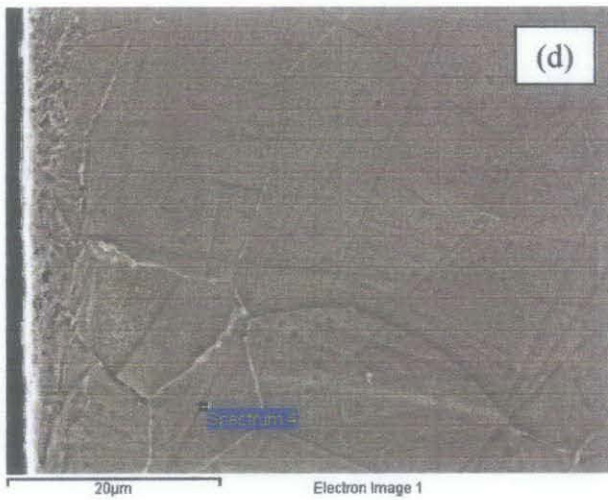
Element	Weight %	Atomic %
Cr	10.51	4.37
N	2.44	3.77



Element	Weight %	Atomic %
Cr	16.96	15.39
N	1.89	8.36



Element	Weight %	Atomic %
Cr	14.06	9.16
N	-0.40	-0.98

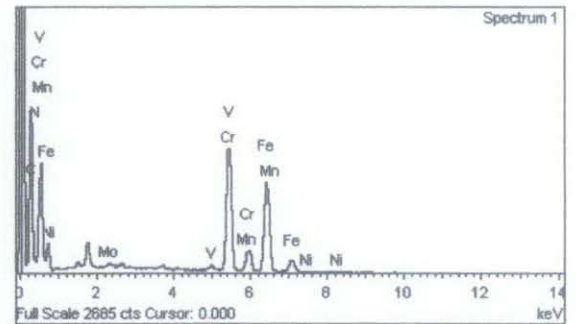
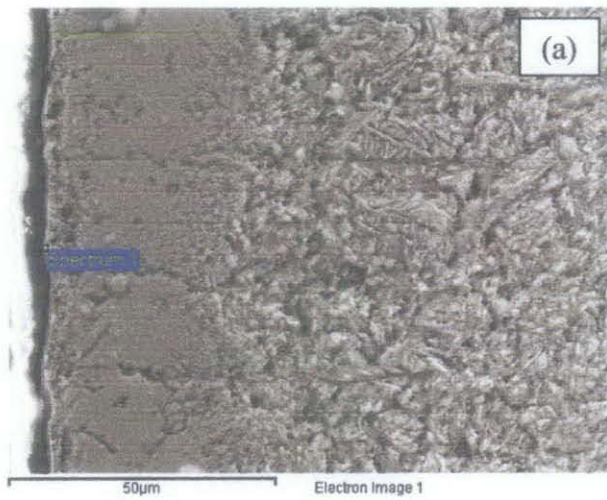


Element	Weight %	Atomic %
Cr	14.19	8.98
N	-0.30	-0.71

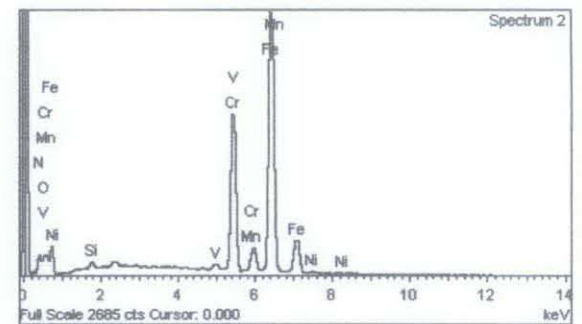
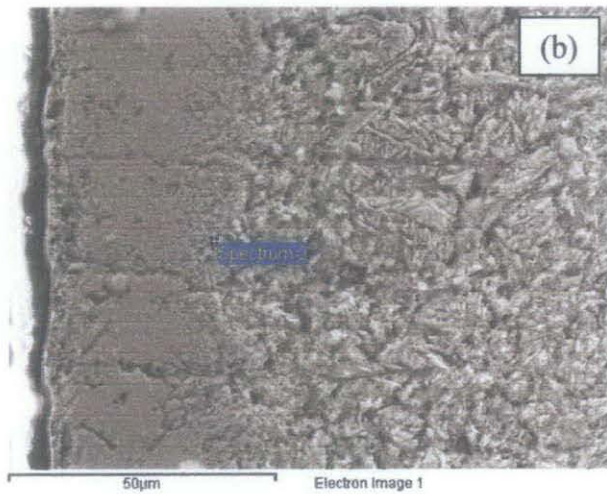
Figure 19: Elemental mapping for austenitic stainless steel after nitriding at 600°C: (a) spectrum 1 (b) spectrum 2 (c) spectrum 3 (d) spectrum 4

4.4.3 9.3%Cr ferritic steel after Nitriding at 900°C

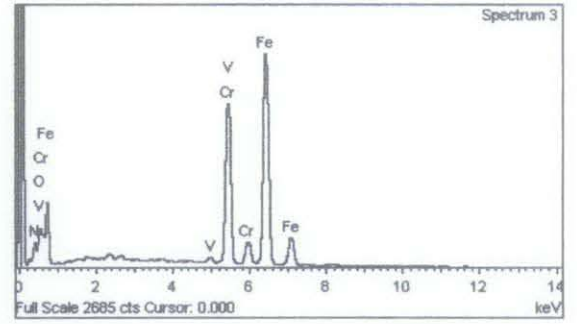
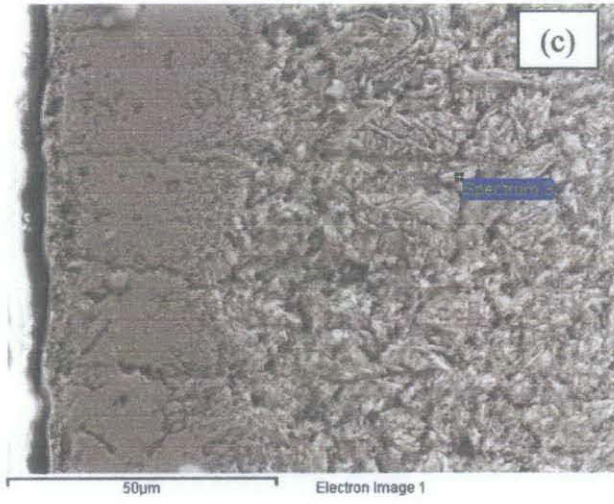
Based on the elemental mapping shown in Figure 20 (a – d), the analysis clearly shown that chromium content start to increase at interface between nitrided layer and diffusion zone. The highest chromium content is at the high depth which is in the diffusion zone (Figure 20 (d)). The nitrogen composition is highest at the surface (Figure 20 (a)) and drop at the transitional area (Figure 20 (b)). In the diffusion zone, the nitrogen composition starts to increase.



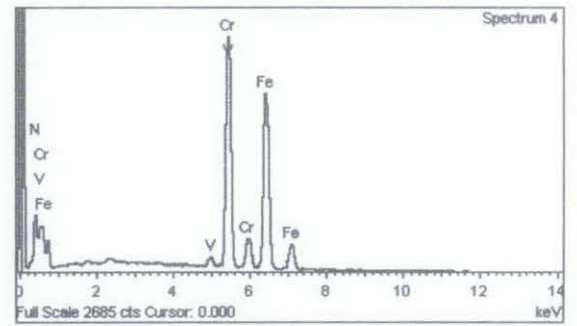
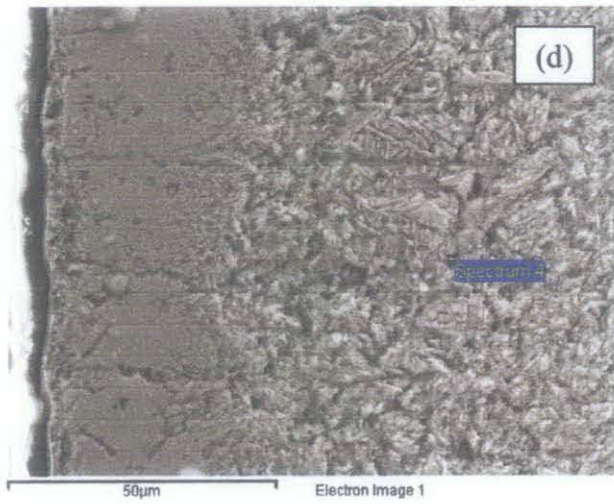
Element	Weight %	Atomic %
Cr	16.54	5.66
N	28.00	35.59



Element	Weight %	Atomic %
Cr	23.53	19.72
N	7.60	23.65



Element	Weight %	Atomic %
Cr	28.12	22.03
N	8.11	23.59



Element	Weight %	Atomic %
Cr	35.31	23.65
N	19.29	47.97

Figure 20: Elemental mapping for 9.3%Cr ferritic steel after nitriding at 900°C: (a) spectrum 1 (b) spectrum 2 (c) spectrum 3 (d) spectrum 4

4.4.4 Austenitic Stainless Steel after Nitriding at 900°C

The highest chromium content is at the interface between nitrided layer and diffusion zone (Figure 21 (b)). The nitrogen composition is increasing along depth (Figure 21 (a–b)).

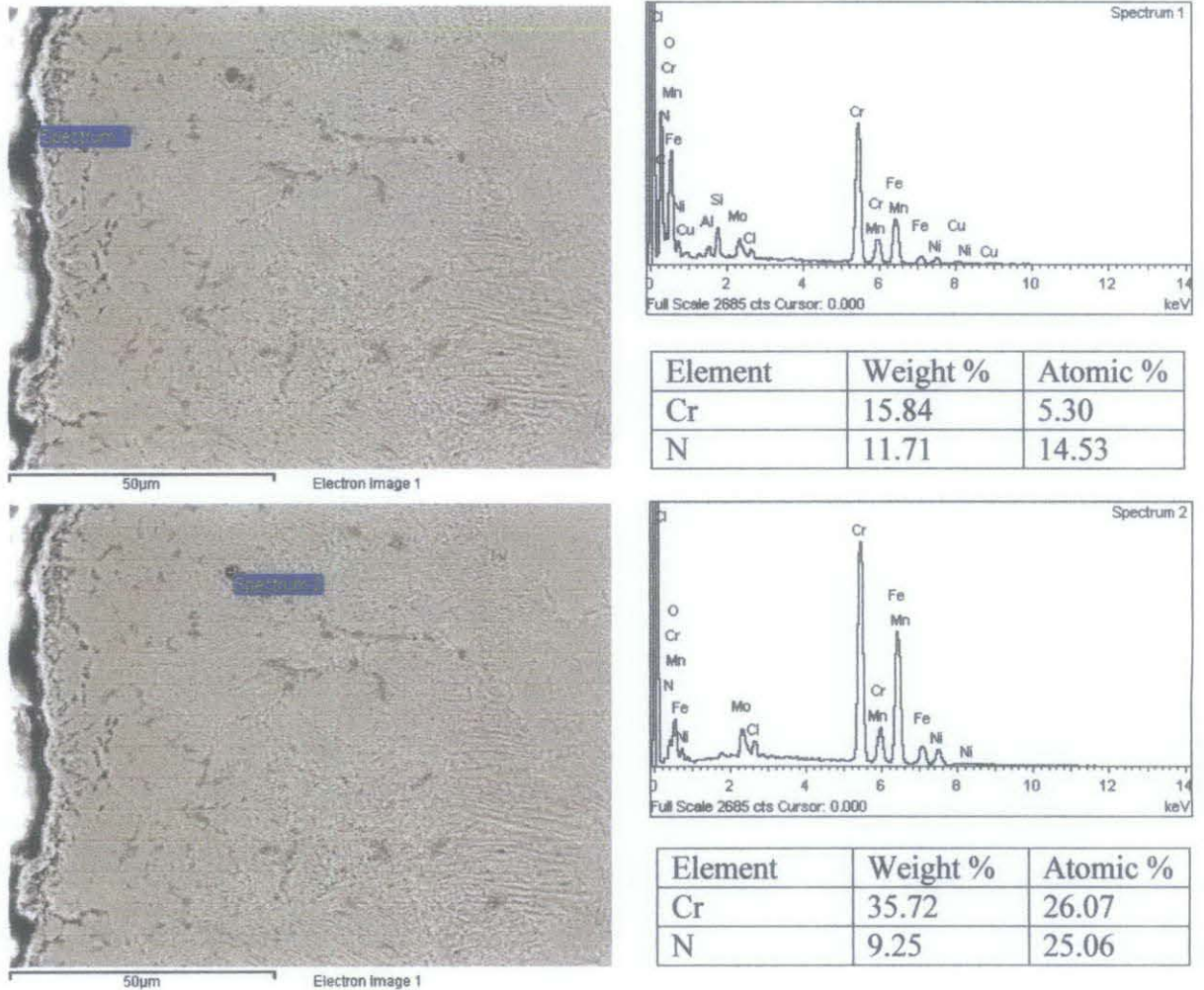


Figure 21: Elemental mapping for austenitic stainless steel after nitriding at 900°C: (a) spectrum 1 (b) spectrum 2

Remarks for Elemental Mapping Analysis of Ferritic Steel and Austenitic 316L

The presence of chromium in nitrided layer and diffusion zone had proved the material had experiencing sensitization effect. The presence of chromium content along the grain boundary also signifies that chromium depletion had occurred after nitriding process. Based on the nitrogen content that had been found during elemental mapping process show us that the diffusion of nitrogen on the material during gas nitriding process. Therefore, the nitriding process had been done successfully.

4.5 UNIVERSAL SCANNING PROBE MICROSCOPY

4.5.1 Surface Topography

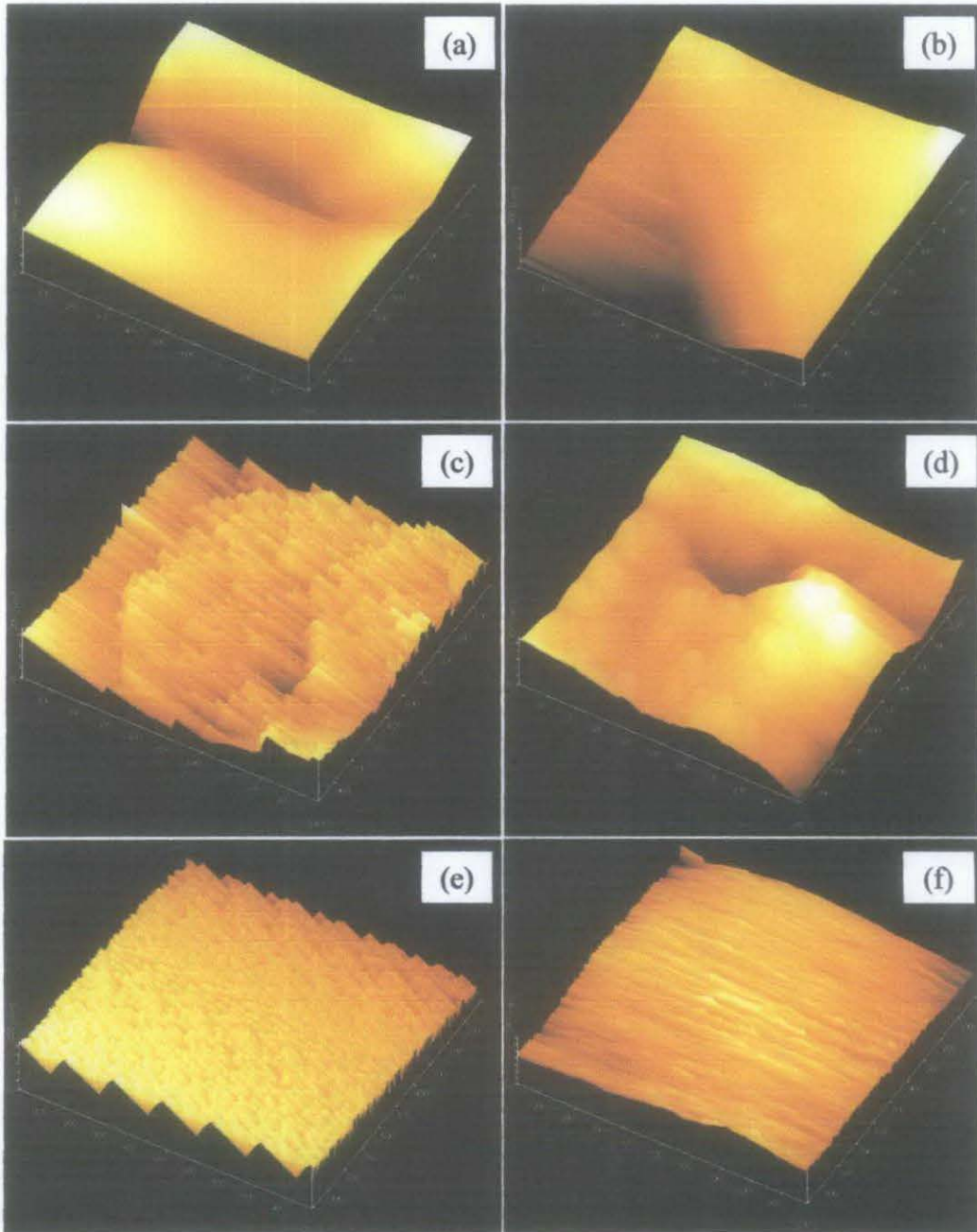


Figure 22: Surface topography of material: (a) nitrided 9.3%Cr ferritic steel at 600°C, (b) nitrided 9.3%Cr ferritic steel at 900°C (c) nitrided austenitic stainless steel at 600°C, (d) nitrided austenitic stainless steel at 900°C (e) untreated 9.3%Cr ferritic steel and (f) untreated austenitic stainless steel

Figure 22 (a – f) shows the surface topography of 9.3% ferritic steel and austenitic stainless steel before and after the treatment. As can be seen in Figure 25, the higher temperature treatment gives a globular product as a result of the deposition process. These results are concurrent with A. Triwiyanto [21] findings.

4.5.2 Surface Phase

The Figure 23 (a-f) shows the phase on surface of the material before and after the nitriding process for 9.3% ferritic steel and austenitic stainless steel.

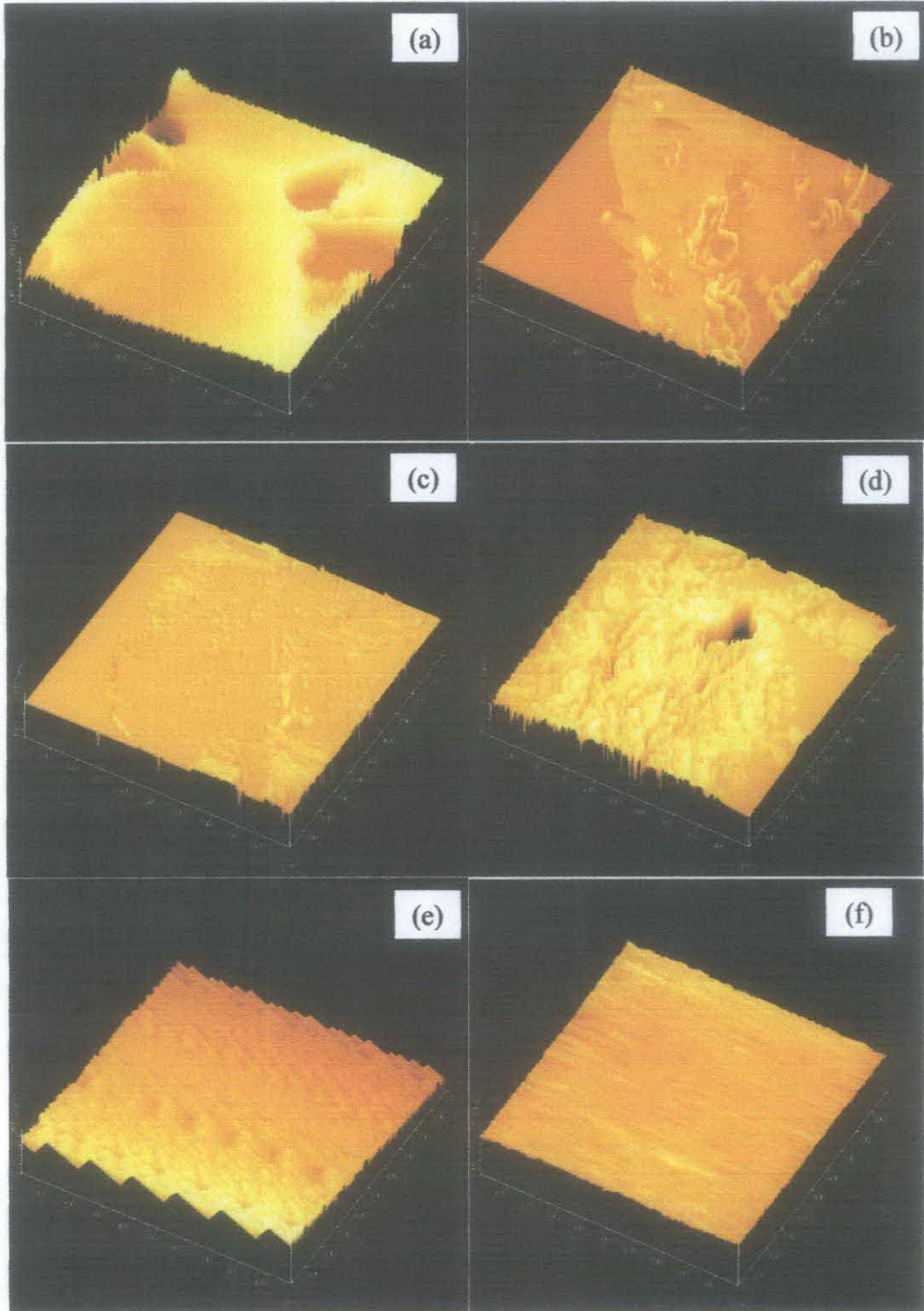


Figure 23: Surface phase of material: (a) nitrided 9.3%Cr ferritic steel at 600°C, (b) nitrided 9.3%Cr ferritic steel at 900°C (c) nitrided austenitic stainless steel at 600°C, (d) nitrided austenitic stainless steel at 900°C (e) untreated 9.3%Cr ferritic steel and (f) untreated austenitic stainless steel

4.5.3 Surface Roughness

The table below shows the roughness average, Ra for untreated and nitrided sample.

Table 5: Roughness Average

Sample	Roughness Average (Ra)	Remarks
Untreated 9.3%Cr ferritic steel	1.593E+01 deg	Figure 24
9.3%Cr ferritic steel after nitriding at 600 ^o C	3.626E+01 deg	Figure 25
9.3%Cr ferritic steel after nitriding at 900 ^o C	9.176E+01 deg	Figure 26
Untreated austenitic stainless steel	1.271E+00 deg	Figure 27
Austenitic stainless steel after nitriding at 600 ^o C	1.369E+01 deg	Figure 28
Austenitic stainless steel after nitriding at 900 ^o C	3.087E+01 deg	Figure 29

According to surface roughness average (Ra) shown in Table 5, the temperature profile will affected the roughness of the surface of material. The higher nitriding temperature, the higher roughness level will be. This is because the size of grain boundary increases as the temperature increase, hence increasing the surface roughness on the material.

Untreated 9.3%Cr Ferritic Steel

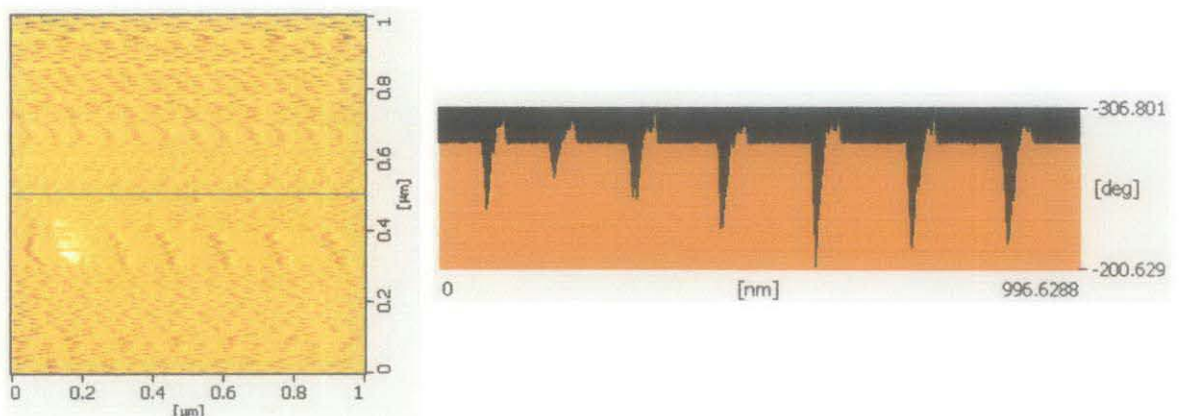


Figure 24: Surface Roughness of Untreated 9.3%Cr ferritic steel

9.3%Cr Ferritic Steel after Nitriding at 600°C

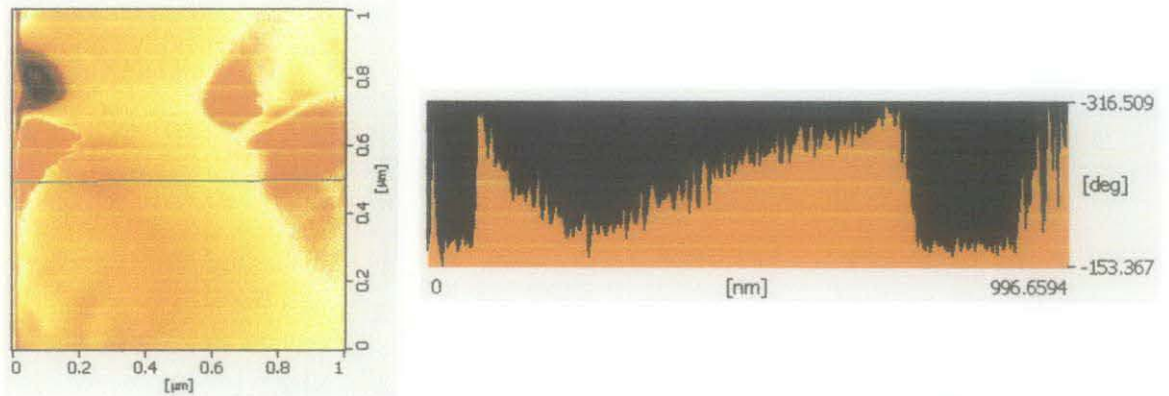


Figure 25: Surface Roughness of Nitrided 9.3%Cr ferritic steel at 600°C

9.3%Cr Ferritic Steel after Nitriding at 900°C

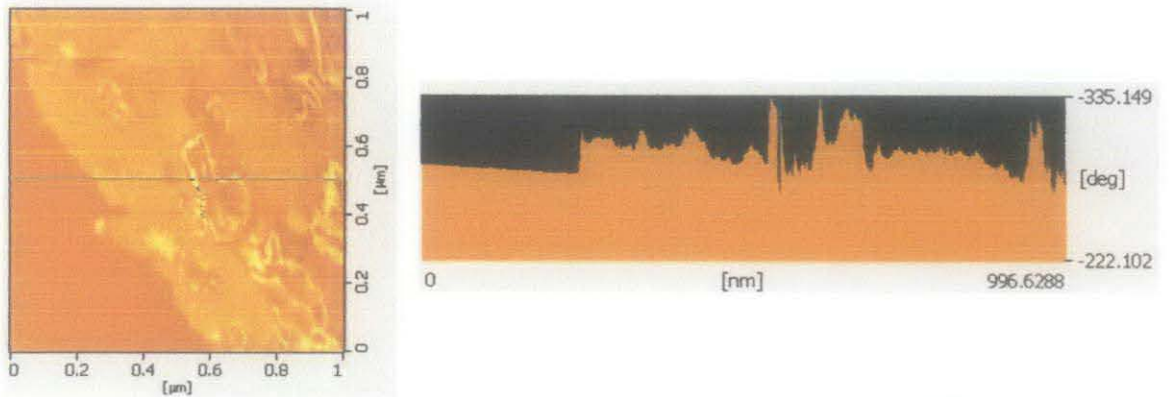


Figure 26: Surface Roughness of Nitrided 9.3%Cr ferritic steel at 900°C

Untreated Austenitic Stainless Steel

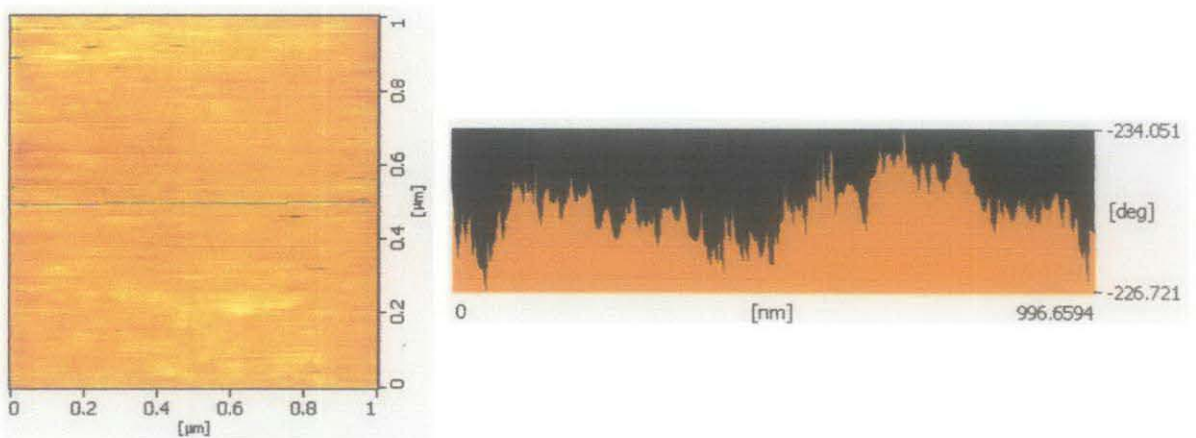


Figure 27: Surface Roughness of Untreated Austenitic Stainless Steel

Austenitic Stainless Steel after Nitriding at 600°C

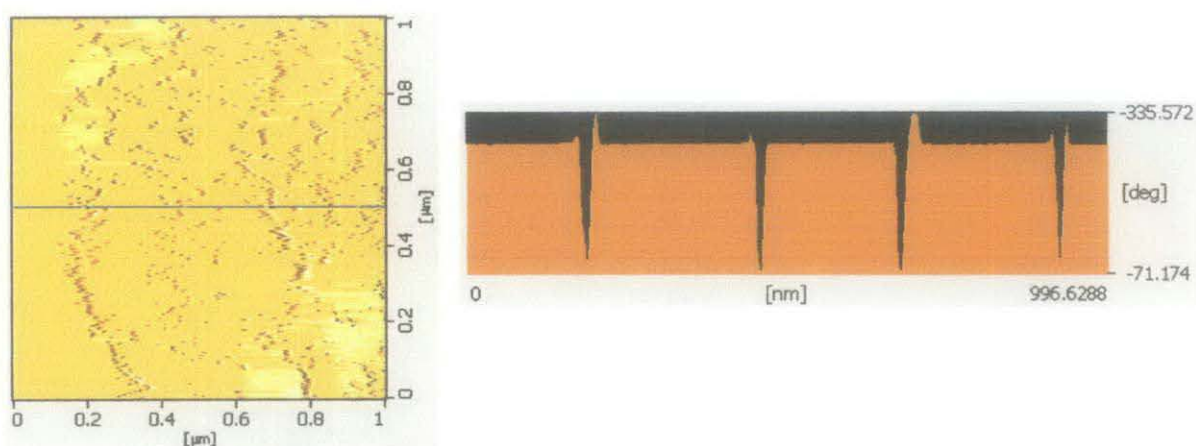


Figure 28: Surface Roughness of Nitrided 9.3%Cr ferritic steel at 600°C

Austenitic Stainless Steel after Nitriding at 900°C

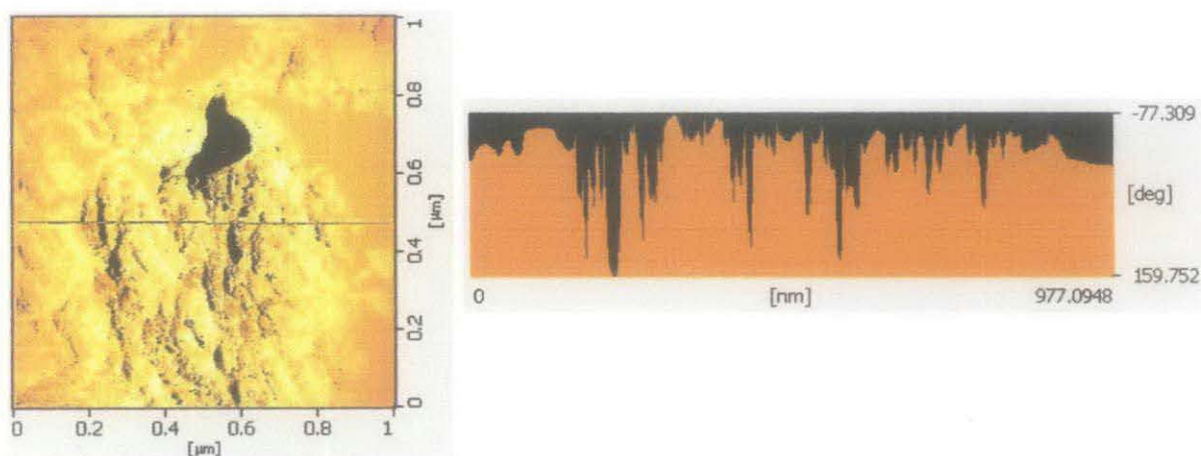


Figure 29: Surface Roughness of Nitrided Austenitic Stainless Steel at 900

4.6 SURFACE MICROHARDNESS

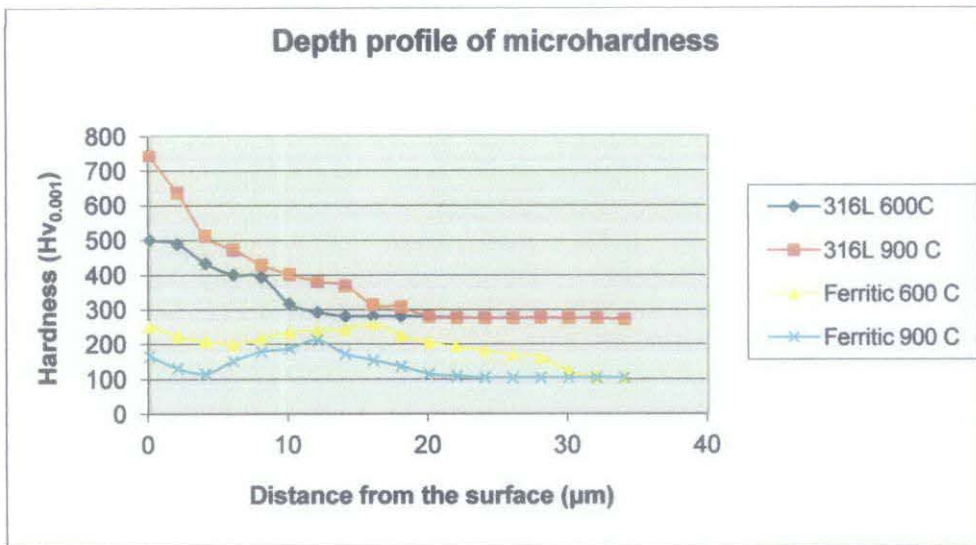


Figure 30: Depth profile of microhardness

Figure 30 shows the hardness depth profiles of the treated specimens. The Nitrided Ferritic steel at 900°C specimen developed a maximum hardness of about 210 Hv about 10µm from the surface, which is much lower than the hardnesses of 741, 394.1 and 257.3 Hv for other three nitrided specimens. The nitrided layer of the 316L at 900°C specimen produced a hard layer of 741.8 Hv with an abrupt layer–core interface, while the nitrided 316L at 600°C produced a gradually decreased hardness profile.

Two Nitrided Ferritic steel specimens, Ferritic 600°C and 900°C developed a similar tendency to fluctuate in hardness profiles at inner nitrided layer as shown in Figure 30 which is related to the behaviour of nitrogen when it diffuse to white layer and diffusion zone as shown in the SEM micrograph in previous section. The most gradual decrease in hardness from 394.1Hv level to substrate hardness was displayed by the nitrided 316L at 600°C specimen but it has thinner layer than nitrided 316L at 900°C.

Remarks on Hardness Profile of Nitrided specimens

1. The hardness profile of Ferritic specimen at 900°C shows the lowest hardness profile compared to other specimens.
2. The hardness profile of Ferritic specimen at 600°C shows higher hardness profile compared to Ferritic at 900°C.
3. The highest hardness profile nitrided of 316L is at 900°C shows different response of nitriding process with hardness profile of nitrided Ferritic steel at the same temperature.
4. Two Nitrided Ferritic steel specimens, Ferritic 600 and 900°C developed a similar tendency to fluctuate in hardness profiles at inner nitrided layer as shown in Fig. 33 which is related to the behaviour of nitrogen when it diffuses to form white layer and diffusion zone.
5. Different type of steel and its composition will give different response to the hardening effect after nitriding process.

CHAPTER 5: CONCLUSION AND RECOMMENDATIONS

5.1 CONCLUSION

In this study, the hardening layer had been successfully produced using the gas nitriding process at 600°C and 900°C. High nitriding process is proven to be one of the heat treatment methods in order to produce expandable austenite layer and hardening layer for 9.3Cr steel. The hardening layer presence had been investigated using optical microscope and FESEM and it can be clearly seen especially under SEM morphology analysis. The presence of hardening layer on the 316L austenitic stainless steel is because the formation of expanded austenite as metastable phase. The chemical reaction during high temperature gas nitriding had created the layer on the ferritic steel. The material properties also had changed after the nitriding process which is being shown in elemental analysis in FESEM-EDS.

There is chromium depletion on both of the sample as we can see the content of chromium increase in the grain boundary during the elemental mapping analysis. Therefore, it is concluded that 316L austenitic stainless steel and 9.3% Cr ferritic steel experiencing sensitization at 600°C and 900°C. Based on the 3D USPM analysis, this study had found out that surface topography of nitrided sample had change its grain size as the temperature increase. The average roughness (Ra) values of material also increase as the nitriding increases according to USPM roughness analysis. This is because the expanded layer formed during the nitriding process is not uniform, hence created different layer depths. The hardness of 316L austenitic stainless steel and 9.3%Cr ferritic steel had been significantly improved after nitriding process. The hardness values of the materials increased as the nitriding temperature increased for 316L austenitic stainless steel and 9.3%Cr ferritic steel.

5.2 RECOMMENDATION

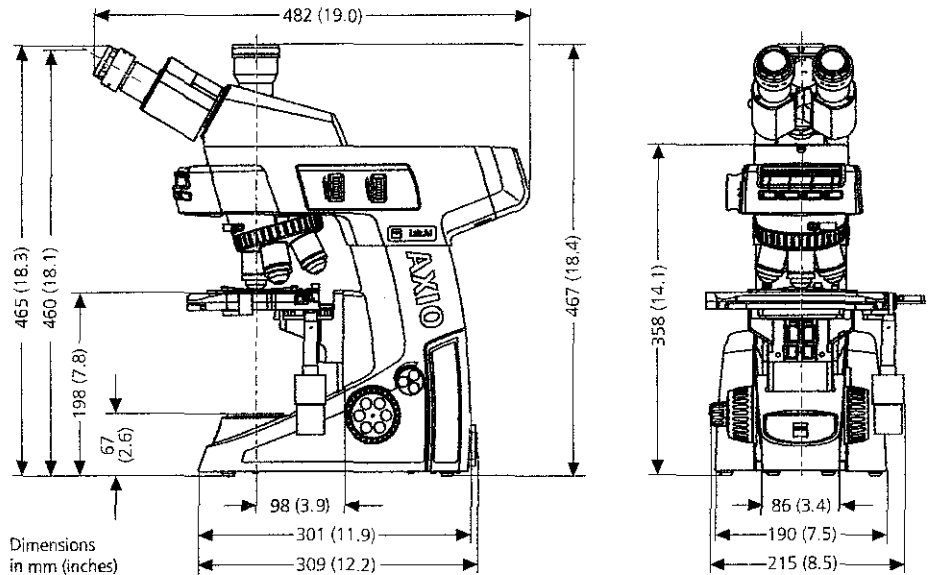
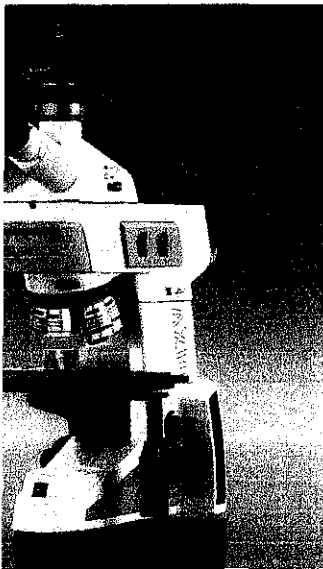
From this research, there are some aspects that need to be carried out in order to enhance the understanding on high temperature nitriding process of 316L austenitic stainless steel and 9.3%Cr ferritic steel using gas nitriding technique. Low temperature gas nitriding process can be done in future in order to study the difference between high temperature nitriding process and low temperature gas nitriding process in terms of sensitization and gas diffusion. The corrosion behavior of the samples also needs to be explored to search for the optimum treatment parameter of gas composition, temperature and time durations according to the industrial requirement. Besides that, further characterization methods towards the substrate after the thermochemical treatments also need to be investigated such as magnetic test, nano-impact and nano-scratch properties on the transition layers. It is important in order to understand the characteristic of austenitic stainless steel and 9.3% Cr ferritic steel as well as its advantages. Lastly, the next research should study on the effect of different types of nitriding process using same methodology of this research.

REFERENCES

- [1] J.D. Redmond and R. M. Davidson, *High Performance Stainless Steel*, Technical Marketing Resources, Inc, Pittsburgh, USA.
- [2] D. Pecker and I. M. Bernstein, *Handbook of Stainless Steel*, McGraw Hill, New York, NY, USA, 1977.
- [3] Atlas Specialty Metals, "Stainless Steel - Grade 316L - Properties, Fabrication and Applications" 2011, <http://www.azom.com/article.aspx?ArticleID=2382>
- [4] Ashok K. Khare, *Ferritic steels for high-temperature applications*, American Society for Metals. N.W., Pennsylvania, October 1981
- [5] Baba H, Kodama T, Katada Y, "Role of nitrogen on the corrosion of behaviour of austenitic stainless steels" *Corrosion science*, vol.1, 2002
- [6] Balaji.S, Vijay.P and Upadhyaya.A, "Effect of Sintering Temperature on the Electrochemical, hardness and tribological properties of aluminide reinforced austenitic stainless steel", *Scripta Materialia*, 2007, pp.1-4.
- [7] Ernest L. and Clyde L, "Chromium Depletion in Vicinity of Carbides in Sensitized Austenitic Stainless Steel", *Metallurgical Transactions A*, vol 15A, May 1984, pp 793
- [8] Christopher F.W, "A Study of Chromium Carbide Precipitation at Interphase Boundaries in Stainless Steel Weld", *University of California, USA*, 1990
- [9] Demo. J.J, "Structure, Constitution and General Characteristic of Wrought Ferritic Stainless Steels", *S.T.P. 619, ASTM, West Conshohocken, Pennsylvania, USA*

- [10] H. Berns, S. Siebert, *ISIJ International* 36 (1996) 927–931.
- [11] A.P. Tschiptschin, A. Toro, surface properties of HNS, in: M. Speidel, C. Kowanda, M. Diener (Eds.), *HNS 2003—High Nitrogen Steels*, Hochschulverlag, Zurich, 2003, pp. 229–240.
- [12] V.G. Gavriljuk, H. Berns, *High Nitrogen Steels*, Springer-Verlag, Berlin, 1999, p. 378.
- [13] E.C Bain, R.H. Aborn and J.B Rutherford, *Trans. Am. Steel Treating*, 21(1933) pg481
- [14] C. Strawstorm and M. Hillert, *J. Iron Steel Institute*, 207 (1969) pg 77-85
- [15] Lewis M.H. and Hattersley B. “Precipitation of $M_{23}C_6$ in Austenitic Steels”. *Acta Metall.*, 13:1159-1168, 1965.
- [16] Tanaka H., Murata M., Abe F., and Yagi K. “The Effect of Carbide Distributions on long-term Creep Rupture Strength of SUS321H and SUS347H stainless steels”. *Mater. Sci. Eng.*, A234:1049-1052, 1997.
- [17] Fontana, M.G., *Corrosion Engineering*, 3rd Ed, McGraw-Hill, New York, 1987
- [18] V. Muthukumar, V. Selladurai, S. Nandhakumar, M. Senthilkumar, “Experimental investigation on corrosion and hardness of ion implanted AISI 316L stainless steel,” *J. of Material Design*, 31, p. 2813-2817. 2010.
- [19] X-ray diffraction analysis of nanoparticles: recent developments, potential problems and some solutions Whitfield, P.; Mitchell, L. Dec 2004.
- [20] O. O’zturk and D.L. Williamson, Phase and Composition Distribution Analyses of Low Energy High Flux N Implanted Stainless Steels, *J. Appl. Phys.*, 1995, 77, p 3839–3851.

[21] A. Triwiyanto, “Structural and Properties Development of Expanded Austenite Layers on AISI 316L after Low Temperature Thermochemical Treatments”, *J. Appl. Phys.*, 2011.



Axio Lab.A1 – Technical Data

Stand	Upright microscope Axio Lab.A1 integrated reflected light illumination
Focus	Manual, coaxial coarse/fine drive, 30 mm travel range
Illumination	Halogen reflector lamp HAL 50/12V 50W, optional LED
Nosepiece	5 position nosepiece, for brightfield and darkfield, M27
Reflector turret	4 position for Push&Click modules
Power supply unit	Internal 12V DC 50W stabilized 100...240V AC/50...60Hz/110VA
Filter slider	2 positions; 25 mm diameter
Stage	Mechanical stage, 75x30 mm, coaxial drive right side, anodized surface hardcoated specimen holder included
Eyepieces	PL 10x/20 Br. foc. PL 10x/22 Br. foc.
Camera	AxioCam ERc 5s Sensor: 5 MP CMOS Sensor Resolution: 2560 (H) x 1920 (V) = 5.0 Megapixels Pixel size: 2.2 µm x 2.2 µm Interfaces: 1x SD card slot, 1x mini USB 2.0, 1x AV (S-Video), 1x DVI (HDMI) C-mount

Carl Zeiss MicroImaging GmbH
07740 Jena, Germany

Industrial | Göttingen Location
Phone : +49 551 5060 660
Telefax: +49 551 5060 464
E-Mail : micro@zeiss.de

www.zeiss.de/AxioLab-Mat

Technical Data

Essential Specifications	SUPRA 40VP	SUPRA 55VP	SUPRA 60VP
Resolution (optimal WD) <i>All resolution specifications are dependent on the system configuration.</i>	1.0 nm @ 15 kV 1.9 nm @ 1 kV 2.0 nm @ 30 kV (VP mode)		0.8 nm @ 15 kV 1.6 nm @ 1 kV 2.0 nm @ 30 kV (VP mode)
VP Vacuum	2 - 133 Pa, adjustable in steps of 1 Pa		
Magnification	12 - 1,000,000 x		
Emitter	Thermal field emission type		
Acceleration Voltage	0.02 - 30 kV		
Probe Current	Configuration 1: 4 pA - 20 nA / Configuration 2: 12 pA - 100 nA		
Detectors	High efficiency in-lens detector, Everhart-Thornley Secondary Electron Detector, VPSE Detector, Cap mounted AsB [®] detector		
Chamber	330 mm (Ø) x 270 mm (h), 1 EDS port 35° to optical axis, CCD-camera with IR illumination, Additional Znd EDS port 35° to optical axis	330 mm (Ø) x 270 mm (h), 2 EDS port 35° to optical axis, CCD-camera with IR illumination, Chamber for fully focussing WDS spectrometer	520 mm (Ø) x 300 mm (h), 1 EDS port 35° to optical axis, Integrated 8" airlock, CCD-camera with IR illumination
Specimen Stage	5-Axes Motorised Eucentric Specimen Stage X = 130 mm, Y = 130 mm, Z = 50 mm, T = -3 - +70° R = 360° (continuous) 6-Axes Eucentric Stage X = 100 mm, Y = 100 mm, Z = 42 mm, Z' = 13 mm, T = -4 to 70°, R = 360° (continuous)		6-Axes Motorised Super-Eucentric Specimen Stage X = 152 mm Y = 152 mm Z = 43 mm Z' = 10 mm T = -15 - 60° R = 360° (continuous)
Image Processing	Resolution: Up to 3072 x 2304 pixel, Noise reduction: Seven integration and averaging modes		
Image Display	Single 19" TFT monitor with SEM image displayed at 1024 x 768 pixel		
System Control	SmartSEM** with Windows*XP, operated by mouse, keyboard and joystick with optional control panel		
Space Requirement	Minimum footprint: 1.97 m x 1.73 m, Minimum working area: 3.5 m x 5.0 m		Minimum footprint: 2.81 m x 1.73 m, Minimum working area: 3.5 m x 5.0 m
<i>SmartSEM** - Fifth generation SEM control Graphical User Interface</i>			

= upgrades

GANTT CHART

FINAL YEAR PROJECT 1

No	Detail/ Week	1	2	3	4	5	6	7		8	9	10	11	12	13	14	
1	Selection of Project Topic								Mid-Semester Break								
2	Preliminary Research Work																
3	Submission of Extended Proposal						●										
4	Preparation for Oral Proposal Defense										●						
5	Study on Techniques of Thermal Analysis																
6	Submission of Interim Draft Report															●	
7	Submission of Finalized Interim Report																●



● Suggested milestone Process

GANTT CHART

FINAL YEAR PROJECT 2

No.	Detail/ Week	1	2	3	4	5	6	7	8	9	10	11	12	13	14	15	
1	Project Work Continue:																
2	Submission of Progress Report								●								
3	Project Work Continue:																
4	Pre-EDX											●					
5	Submission of Draft Report												●				
6	Submission of Dissertation (soft bound)														●		
7	Submission of Technical Paper														●		
8	Oral Presentation															●	
9	Submission of Project Dissertation (Hard Bound)															●	

Mid-Semester Break

 Suggested milestone
 Process